Section 7

Global and regional climate models, sensitivity and impact experiments, response to external forcing

About Negative Correlations of Surface Temperature and Clouds Parameters for Antarctic Region

Oleg A. Alduchov, Irina V. Chernykh,
Russian Research Institute of Hydrometeorological Information- Word Data Center, Obninsk, Russia,
E-mails: aoa@meteo.ru, civ@meteo.ru

In previous study it was detected, that climatic changes of air surface temperature T in eastern and western part of Antarctica have different tendencies: warming was detected for some stations at the West and cooling was detected for some stations of the East [Comiso, 2000; Marshall et al. 2002, Turner et al., 2004 Chernykh and Alduchov, 2003a, 2003b, Jagovkina et al., 2004]. Clouds play very important role in distribution of solar radiation at the earth surface. But dependence of climate changes of surface temperature and clouds is not very pore. These changes can take place in different layers of the atmosphere. It is known, that distributions of cloud parameters, such as cloud amount, frequencies of cloud types are different for these regions [Warren, et al. 1986]. Increasing of cloud amount (up to 15-20%) at the South Pole, detected by Neff in 1999, was described in the documents of Intergovernmental Panel on Climate Change as “dramatic” [Climate Change, 2001].

Are exist any parameters of clouds which have negative correlations with air surface temperature for stations placed in both eastern and western and central parts of Antarctica, or for one of this part?

These researches are made on base Aerological dataset CARDS [Eskridge et al. 1995] for period 1964-2001 years. The present study is focused on the Eastern Antarctic coastal stations: Novolazarevskaya (89512); Syowa (89532); Molodezhnaya (89542); Mawson (89564); Davis (89571); Mirny (89592); Casey (89611); Dumont D’Urville (89642); Macquarie Island (94998); McMurdo (89002); Western Antarctic coastal stations: Bellingshausen (89050); Base Marambio (89055), Halley Bay (89022); Newmayer (89002); continental Antarctic stations: Amundsen Scott (89009); Vostok (89006).

CE-method was used to determine cloud boundaries and amount from temperature and humidity profiles [Chernykh and Eskridge 1996, Chernykh and Alduchov, 2004]. Correlations $\mu^{ta}{}_{i}$ for time series of monthly averaged means anomalies of cloud parameters and surface temperature for every station were calculated.

Monthly averaged mean values were calculated for five parameters of cloud vertical macrostructure: frequency of cloud layers (Freq), number (NLay) and total thickness (Thic) of cloud layers, base of lowest cloud layer (Base) и top of highest cloud layer (Top). All these parameters were determined for six atmospheric layers: 0-2 km, 2-6 km, 6-10 km (for L - low, M - middle and H – high level of clouds accordingly), and for layers 0-6 km, 2-10 km и 0-10 km about ground level (LM, MH, LMH, соответственно). Calculations were made for five following gradations of cloud amount. Symbols for these gradations present below:

1) 0-20%! – 0-20% of sky coverage independently of presence of any other cloud layers;
2) 20-60%! –20-60% of sky coverage independently of presence of any other cloud layers;
3) 60-80%! – 60-80% of sky coverage independently of presence of any other cloud layers;
4) 80-100%! – 80-100% of sky coverage independently of presence of any other cloud layers;
5) 0-100% – 0-100% of sky coverage (any clouds independently of amount).

So, totally we have 150 (5x6x5) cloud parameters to check correlations with surface temperature.

Calculations have shown that there is no exists any cloud parameter with negative correlations with respect T for all sixteenth. Frequency of middle cloud is one cloud parameter with negative correlations with respect T for all studied Eastern Antarctic coastal stations (see Table 1).

Table 1. Cloud parameter with negative correlations with respect T
for Eastern Antarctic coastal stations (and for fourteenth Antarctic Stations also).

Atmos. layer	Cloud amount	Param. of cloud	Eastern Antarctic coastal stations									
			89512	89532	89542	89564	89571	89592	89611	89642	94998	89664
			Correlations $\mu^{ta}{}_{i}$									
M	0-100%	Freq	-.002	-.256	-.015	-.064	-.027	-.060	-.082	-.246	-.028	-.139

Atmos. layer	Cloud amount	Param. of cloud	Western Antarctic coastal stations				Continental Antarctic stations	
			89050	89055	89022	89002	89009	89606
			Correlations $\mu^{ta}{}_{i}$					
M	0-100%	Freq	.014	-.157	-.019	-.084	.107	-.221

Most important cloud parameter with negative correlations with respect T for Western Antarctic coastal stations is cloud number (see Table 2).

Most important cloud parameter with negative correlations with respect T for continental Antarctic stations is cloud number also (see Table 3).

Table 2. Cloud parameter with negative correlations μ^{ta}_{i} with respect T for four Western Antarctic coastal stations

Atmospheric layer	Cloud amount	Parameter of cloud	Correlations μ^{ta}_{i}			
			89050	89055	89022	89002
H	20-60%!	NLay	-.036	-.183	-.275	-.105
M	0-100%	NLay	-.141	-.082	-.343	-.157
LMH	0-100%	NLay	-.101	-.188	-.480	-.169
H	0-100%	NLay	-.145	-.057	-.539	-.164
LM	0-100%	NLay	-.160	-.136	-.336	-.166
MH	0-20%!	NLay	-.070	-.086	-.253	-.296

Table 3. Cloud parameter with negative correlations with respect T for two continental Antarctic stations

Atmospheric layer	Cloud amount	Parameters of cloud	Correlations μ^{ta}_{i}	
			89009	89606
H	20-60%!	NLay	-.410	-.571
M	0-100%	NLay	-.455	-.337
MH	20-60%!	NLay	-.504	-.137
M	80-100%!	NLay	-.402	-.385
MH	60-80%!	NLay	-.006	-.500

This study is useful to gain insight into climate and climate change in Antarctica and for aviation. Further joint international researches should be very useful. The research was partly supported by RBRF, Project 04-05-64681 and Russian “Study and Investigation of Antarctic” Sub-Program.

References

Climate Change 2001: The Scientific Basis. Contributing of Working Group I to the Third Assessment Report of the Intergovernmental Panel on Climate Change 2001: Cambridge University Press., Cambridge, United Kingdom and New York, NY, USA, 881 p.

Chernykh I. V. and R. E. Eskridge, 1996: Determination of cloud amount and level from radiosonde soundings. *J.Appl. Meteorol, 35,* 1362-1369.

Chernykh I.V., O.A. Alduchov, 2003a: Analysis of Climatic Changes of Cloud Layers Vertical Structure in Atmospheric Layer below 250 hPa in Antarctica. 27 Annual Climate Diagnostics and Prediction Workshop. 21-25 October 2002. Virginia. USA http://www.cpc.ncep.noaa.gov/products/outreach/proceedings/cdw27_proceedings/ichernykh_2002.pdf

Chernykh I.V., O.A. Alduchov, 2003b: Joint Analysis of Climatic Changes of Surface Temperature and Cloudiness Vertical Structure in Antarctic Region on base CARDS. Research Activities in Atmospheric and Oceanic Modelling. WMO. Report No. 33. WMO/TD No 1161. P. 07-05 - 07-06..

Chernykh I.V., Alduchov O.A. 2004: Vertical Distribution of cloud Layers from Atmospheric Radiosonding Data. Izvestiya, Atmoapheric and Oceanic Phisics. V. 40. No 1. P. 45-59.

Comiso J.C. , 2000: Variability and trends in Antarctic surface temperatures from in situ and satellite infrared measurements. J. Climate, **15,** No 10, 1674-1696.

Eskridge, R. E., O. A. Alduchov, I. V. Chernykh, P. Zhai, S. R. Doty, and A. C. Polansky, 1995: A Comprehensive Aerological Reference Data Set (CARDS): Rough and systematic errors. *Bull. Amer. Meteor. Soc.,* **76**, 1959-1775.

Jagovkina S.V., Alduxov O.A., Chernykh I.V., Lagun V.E. 2004. Antarctic free atmosphere parameters variability diagnosis. SCAR Open Science Conference, 26-28 July 2004, Bremen, Germany. Abstract: S16/P.07, p. 371.

Marshall G.J., Lagun V.E., Lachlan-Cope T.A. 2002: Changes in Antarctic Peninsula tropospheric temperatures from 1956-99: a synthesis of observations and reanalysis data // International Journal of Climatology. V. 22, pp. 291-310.

Neff, W.D. 1999: Decadal time scale trends and variability in the tropospheric circulation over The South Pole. J. Geophys. Res., 104(D22), 27217-27251

Turner J., Colwell S.R., Harangozo S.A. 1997: Variability of precipitation over the coastal Antarctic Peninsula from synoptic observations. J. Geophysical research, V. 102. P. 13999-14007.

Turner J., Colwell S.R., Marshall J., Lachlan-Cope T., Carleton A.M., Jones P.D, Lagun V.E, Reid P.A., Jagovkina S. 2004. The SCAR READER project: Towards a high-quality data base of mean Antarctic meteorological observations. Journal of Climate.V.17, N.14, pp. 2890–2898.

Warren, S.G., C.J. Hahn, J. London, R.M. Chervin, and R.L. Jenne 1986: Global distribution of total cloud cover and cloud type amounts over land. NCAR Tech. Note NCAR/TN-273 + STR. 29p. plus 200 maps.

CHANGES IN PRECIPITATION INTENSITY UNDER CLIMATE CHANGE CONDITIONS OVER MAJOR CATCHMENTS IN EUROPE

Katharina Bülow, Daniela Jacob, Ralf Podzun
Max-Planck-Institute for Meteorology, Bundestr. 53, 20146 Hamburg, Germany, buelow@dkrz.de

INTRODUCTION

During the last 10 to 15 years extreme weather events seem to appear more often and sometimes intensified in Europe. The severe drought connected to a heat waves in summer 2003 covered large parts of southern and central Europe. The time period June-August 2003 was up to 5 °C warmer then the 1961-90 average, making 2003 the warmest summer in the above mentioned area since at least 1864 (Fink, 2004, Schaer et al 2004, Bader, 2003).
Extreme precipitation, defined as days with more than 30 mm precipitation, can lead to devastating land-slides and to summer flooding like the Elbe flooding in August 2002.
Precipitation was observed at Hohenpreissenberg, Germany since 1879. The annual precipitation sum shows an increasing trend. The temperature increases around 0.9 °C at Hohenpreissenberg and around 0.6 °C in the mean in Germany in the 20. Century (www.dwd.de/research/mohp/hp2/gaw/gaw.htm).

MODEL AND EXPERIMENTS

The three-dimensional hydrostatic climate model REMO (REgional MOdel (Jacob, 2001)) was used to study the hydrological cycle over Europe, with special focus on the Elbe and Rhine drainage basins. To address the reliability of climate change studies it is important to analyze a set of three regional simulations: for today's climate, control and future climate. For all experiments REMO, version 5.1, using the physical parameterization schemes from the global climate model ECHAM4 was run on 0.5° as well as on 0.16° horizontal resolution covering Europe. For today's climate REMO has been driven at the lateral boundaries by re-/analyses data from ECMWF, the so-called perfect boundaries, to investigate the quality of the REMO results through a detailed comparison against observations, which turned out to be in very good agreement (Milliez, 2003).

To investigate the influence of climate change on the hydrological cycle concentrations of greenhouse gases and sulphate aerosol are chosen according to IPCC (International Panel on Climate Change Scenario) scenario B2 (Houghton, 2001). Two more experiments are necessary: a control run and a scenario run. The difference between these results can be attributed to the climate change signal. Data from the coupled global climate model system ECHAM4-OPYC3 have been used to drive REMO on 0.5° horizontal resolution, which in turn was used as lateral boundaries for REMO 0.16° horizontal resolution.

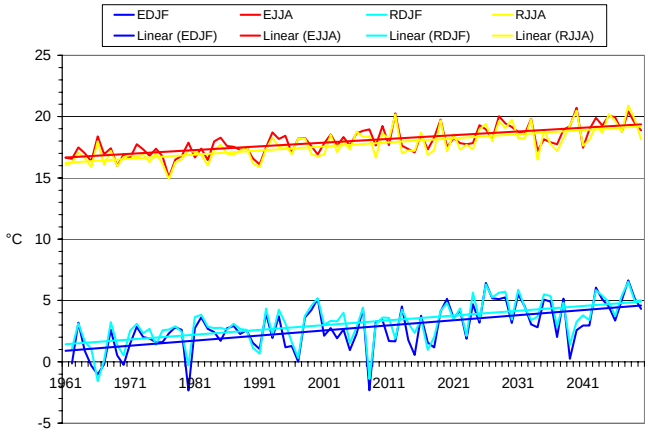

Figure1: Rhine and Elbe drainage basins: seasonal mean Temperature (REMO 5.1, 0.16 °, SRES B2)

RESULTS

In the period 1961-2050, the mean summer (JJA) temperature will rise around 2-3 °C in both drainage basins (Figure 1). The winter temperature (DJF) will rise at least around 3 °C. The variability of the mean winter temperatures are greater (~5 °C) than of the summer temperatures (~3 °C).

The daily precipitation intensities of the Elbe drainage basin show a clear increase from more than 5 % (10-20 mm) in the winter (DJF), but do not show any significant changes in the summer (JJA).

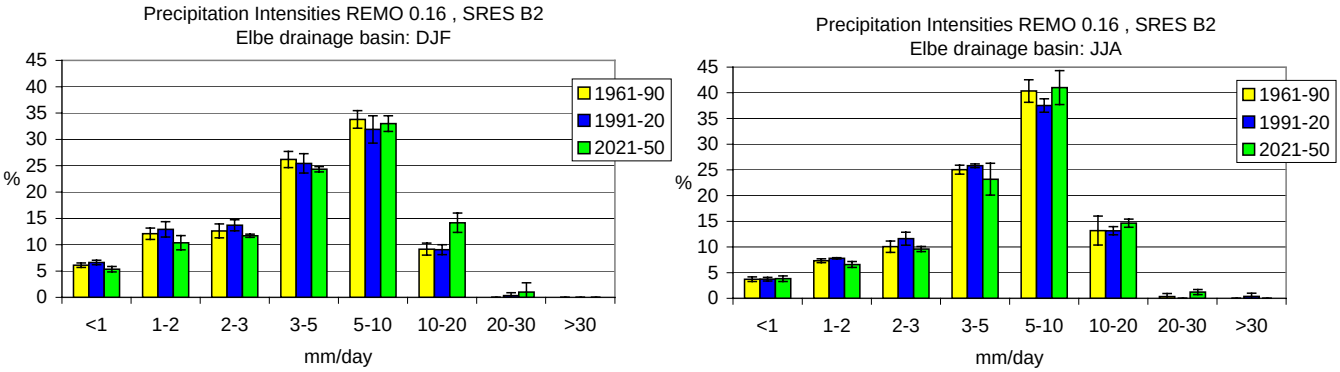

Figure 2: Simulated precipitation intensities (mm/day) for the Elbe basin (REMO 5.1, 0.16 °, SRES B2)

ACKNOWLEDGEMENT

Parts of the work have been carried out within the BMBF-funded project GLOWA-ELBE as well as within KLIWA project, funded by three GERMAN water management agencies.

REFERENCES

Bader, S. and Zbinden, L. (2003): Aussergewoehnlicher Hitzerekord. MeteoSchweiz report, http://www.meteoschweiz.ch/de/Wissen/Rekorde/ tempMaxJuni03.shtml

Fink, A., Bruecher,T., Krueger,A., Leckebusch,G, Pinto, Joaquim, Ulbrich,U. (2004): The 2003 European summer heatwaves and dought – synoptic diagnosis and impacts, Weather – August 2004, Vol.59, No.8, 209-214.

Houghton, J.T et al., (2001): Climate Change 2001: The Scientific Basis, Contribution of Working Group I to the Third Assessment Report of the Governmental Panel on Climate Change, Cambridge University Press.

Jacob, D., (2001): A note to the simulation of the annual and interannual variability of the water budget over the Baltic Sea drainage basin, Meteorol. Atmos. Phys.77, p. 61-73.

Jacob, D., Van den Hurk, B.J.J.M., Andræ, U., Elgered, G., Fortelius, C. Graham, L. P., Jackson, S.D., Karstens, U., Koepken, Chr., Lindau, R., Podzun, R., Roeckel, B., Rubel, F., Sass, B. H., Smith, R.N.B.,

Milliez, M. (2003): Validation of today's climate simulation with the regional model REMO. Diplomarbeit am DEA Oceanologie, Meteorologie et Environnement, der Universite Pierre et Marie Curie.

Schär, C., P.L. Vidale, D. Lüthi, C. Frei, C. Häberli, M. Liniger and C. Appenzeller, 2004: The role of increasing temperature variability in European summer heatwaves. Nature, 427, 332-336; doi:10.1038/nature02300

About Climatic Changes of Clouds and Precipitation over Antarctic Peninsula

Irina V. Chernykh, Oleg A. Alduchov,
Russian Research Institute of Hydrometeorological Information- Word Data Center, Obninsk, Russia,
E-mails: civ@meteo.ru , aoa@meteo.ru
and Victor E. Lagun,
Arctic and Antarctic Research Institute, St. Petersburg, Russia
E-mails: lagun@aari.nw.ru

Antarctic Peninsula is a region with good known warming [Comiso, 2000; Marshall et al. 2002, Turner et al., 2004]. In previous study it was founded, that air surface warming over Antarctic Peninsula takes place together with changes in sea ice extent, changes in main atmospheric parameters in troposphere (warming in the troposphere, increasing of water vapor amount observed from 850 hPa, decreasing of wind speed at surface level and in troposphere), increasing of cyclone frequency and changes of cloudiness vertical macrostructure (in atmospheric layer 0-10 km for cloud layers with cloud amount 0-100% of the sky there was detected an increasing of total thickness; decreasing of cloud layers number; clouds high boundary is decreasing; low boundaries decrease) [Alduchov et al., 2003]. More detailed study of climatic changes of low boundary of cloudiness (LB) for atmospheric layers 0-2 km, 2-6 km, 6-10 km, 0-10 km for different cloud amount 0-20%. 0-60%, 0-80%, 0-100% of the sky was presented for all seasons and for year in paper [Chernykh et al., 2003]. It was founded that low boundaries for clouds with amount 0-100% of the sky in atmospheric layers 0-2 km and 0-10 km for Bellinsgshausen decrease with decadal changes of –35 m/decade and –66 m/decade accordingly. Researches was made for Russian station Bellinsgshausen, placed near Antarctic Peninsula, because warming for this station was detected by surface, sonde and satellite observations [Comiso J.C., 2000; Chernykh and Alduchov, 2003a, 2003b, Jagovkina et al., 2004]. Increasing of number of reports about precipitation over the coastal Antarctic Peninsula from synoptic observations was founded for Australian winter [Turner et al., 1997]. Existence of cloudiness with cloud amount 80-100% of the sky is necessary condition for exist of precipitation. Which kinds of climatic changes of vertical macrostructure parameters of cloud layers with cloud amount 80-100 % can be detected from data about temperature and humidity profiles obtained on base standard radiosounding of atmosphere ?

Researches are made on base Aerological dataset CARDS (Eskridge et al. 1995) for period 1970-1999 years. CE-method was used to determine cloud boundaries and amount from temperature and humidity profiles [Chernykh and Eskridge 1996, Chernykh and Alduchov, 2004]. Trends in anomalies for all parameters were calculated by linear regression with using measured values with provision for correlation dependence in time.

Trends in anomalies of the frequency and low boundary of cloud layers with cloud amount 80-100% of the sky for atmospheric layers 0-2 km, 2-6 km, 6-10 km, 0-6 km, 2-10 km and 0-10 km are shown on figure 1. Highest increasing (towards other months) of low clouds frequency with decadal changes of 11.8 %/decade is detected for June. Increasing of the frequency of clouds in atmospheric layers 0-6 km and 0-10 km are detected for June also with decadal changes of 7 %/decade and 2.2 %/decade accordingly. Highest increasing (towards other seasons) of frequency of low clouds and clouds in atmospheric layers 0-6 km is detected for summer (Australian winter) with decadal changes of 7.4 %/decade and 3 %/decade accordingly. The frequencies increasing of low clouds and clouds in atmospheric layers 0-6 km for year take place with decadal changes of 4.0 %/decade and 1.4 %/decade accordingly.

It was founded that for summer months low boundaries for clouds with amount 80-100% of the sky in atmospheric layers 0-2 km increase with decadal changes of 20 m/decade for July and decrease with decadal changes –18 m/decade for August. Figure 1 have shown decreasing of low boundaries for clouds in atmospheric layers 2-6 km for all summer month with decadal changes -214 m/decade, -25 m/decade and -60 m/decade for June, July and August accordingly.

These results, obtained on base aerological data, are in agreement with results about increasing of number of reports about precipitation during of Australian winter, obtained on base synoptic observations [Turner et al., 1997] and increasing of cyclone frequency, detected on base twice-daily NCEP/NCAR surface pressure re-analysis data for 1980-1999 [Alduchov et al., 2003].

This study is useful to gain insight into climate and climate change in Antarctica and for aviation. Further joint international researches should be very useful (Turner et al, 2004). The research was partly supported by RBRF, Project 04-05-64681 and Russian “Study and Investigation of Antarctic” Sub-Program.

References

Alduchov O.A., Lagun V. E., Chernykh I.V. 2003: About Climatic Changes of Free Atmosphere Parameters and Cyclonic Activity over Antarctic Peninsula. Word Climate Change Conference. 29 September- 3 October 2003, Moscow, Russia. Abstracts. P. 367.
Chernykh I. V. and R. E. Eskridge, 1996: Determination of cloud amount and level from radiosonde soundings. *J.Appl. Meteorol, 35,* 1362-1369.

Chernykh I.V., O.A. Alduchov, 2003a: Analysis of Climatic Changes of Cloud Layers Vertical Structure in Atmospheric Layer below 250 hPa in Antarctica. 27 Annual Climate Diagnostics and Prediction Workshop. 21-25 October 2002. Virginia. USA http://www.cpc.ncep.noaa.gov/products/outreach/proceedings/cdw27_proceedings/ichernykh_2002.pdf
Chernykh I.V., O.A. Alduchov, 2003b: Joint Analysis of Climatic Changes of Surface Temperature and Cloudiness Vertical Structure in Antarctic Region on base CARDS. Research Activities in Atmospheric and Oceanic Modelling. WMO. Report No. 33. WMO/TD No 1161. P. 07-05 - 07-06..
Chernykh I.V., Alduchov O.A., Lagun V.E., 2003: About Cloudiness Low Boundary over Antarctic Peninsula. Research Activities in Atmospheric and Oceanic Modelling. WMO. Report No. 33. WMO/TD No 1161. P. 02-01 - 02-02. http://www.cmc.ec.gc.ca/rpn/wgne/
Chernykh I.V., Alduchov O.A. 2004: Vertical Distribution of cloud Layers from Atmospheric Radiosonding Data. Izvestiya, Atmoapheric and Oceanic Phisics. V. 40. No 1. P. 45-59.
Comiso J.C. , 2000: Variability and trends in Antarctic surface temperatures from in situ and satellite infrared measurements. J. Climate, **15,** No 10, 1674-1696.
Eskridge, R. E., O. A. Alduchov, I. V. Chernykh, P. Zhai, S. R. Doty, and A. C. Polansky, 1995: A Comprehensive Aerological Reference Data Set (CARDS): Rough and systematic errors. *Bull. Amer. Meteor. Soc.*, **76**, 1959-1775.
Jagovkina S.V., Alduxov O.A., Chernykh I.V., Lagun V.E. 2004. Antarctic free atmosphere parameters variability diagnosis. SCAR Open Science Conference, 26-28 July 2004, Bremen, Germany. Abstract: S16/P.07, p. 371.
Marshall G.J., Lagun V.E., Lachlan-Cope T.A. 2002: Changes in Antarctic Peninsula tropospheric temperatures from 1956-99: a synthesis of observations and reanalysis data // International Journal of Climatology. V. 22, pp. 291-310.
Turner J., Colwell S.R., Harangozo S.A. 1997: Variability of precipitation over the coastal Antarctic Peninsula from synoptic observations. J. Geophysical research, V. 102. P. 13999-14007.
Turner J., Colwell S.R., Marshall J., Lachlan-Cope T., Carleton A.M., Jones P.D, Lagun V.E, Reid P.A., Jagovkina S. 2004. The SCAR READER project: Towards a high-quality data base of mean Antarctic meteorological observations. Journal of Climate.V.17, N.14, pp. 2890–2898.

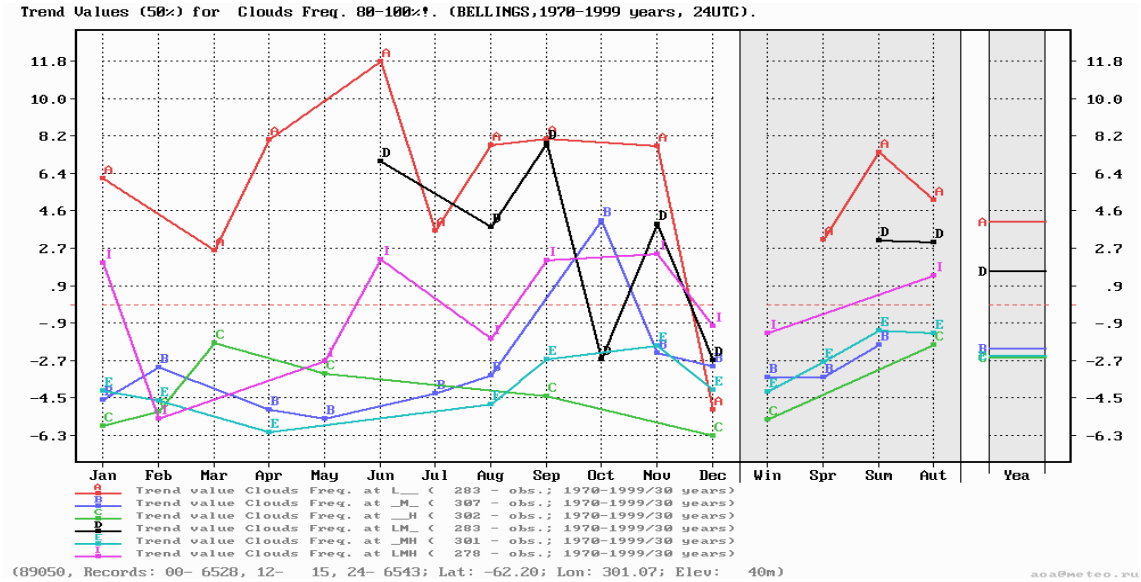

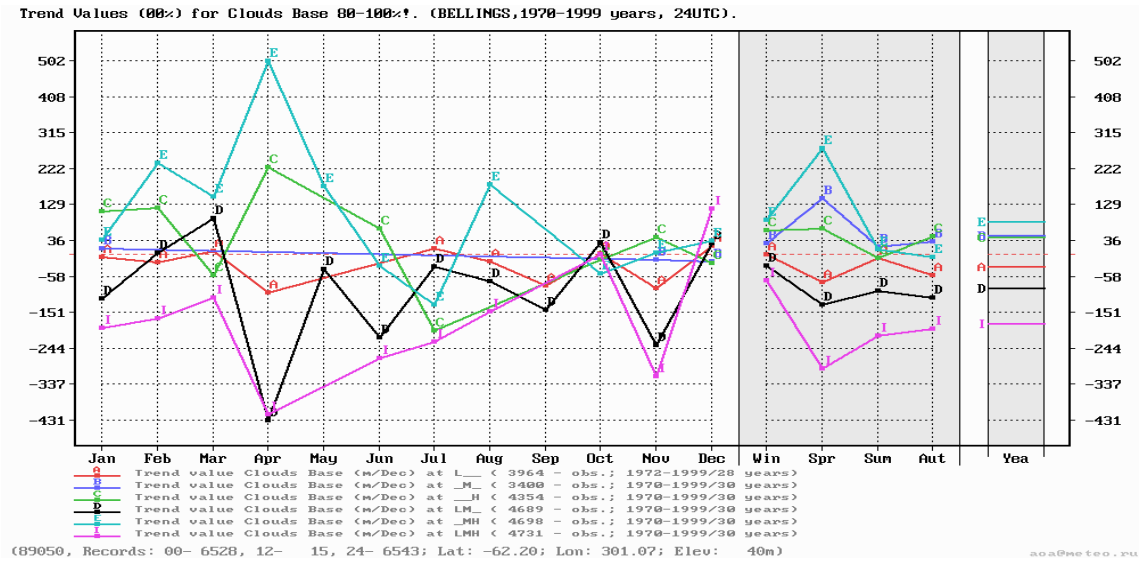

Figure 1. Trends in anomalies of the frequency (on the top of the figure) and low boundary (on the bottom of figure) of cloud layers with cloud amount 80-100% of the sky for atmospheric layers 0-2 km (A), 2-6 km (B), 6-10 km (C), 0-6 km (D), 2-10 km (E), 0-10 km (I) for all month (on the left) season (in centre) and year (on the right) for Bellingshausen. 1970-1999 years. Win – December-February. CARDS. Trends in anomalies were calculated by linear regression with using measured values with provision for correlation dependence in time. Trends were detected with significance level not less than 50%.

Time-lagged Effects of Spring Tibetan Plateau Soil Moisture on the Monsoon over China in Early Summer

K. C. Chow and Johnny C. L. Chan
Department of Physics & Materials Science, City University of Hong Kong.
e-mail: apkchow@cityu.edu.hk

It has been shown in numerous studies that a clear relationship exists between the amount of winter or spring snow over the Tibetan Plateau (TP) and the rainfall over the Yangtze River region (YR) in eastern China and the south China region (SC) in the subsequent summer (e.g. Wu and Qian 2003; Qian et al. 2003; Zhang et al. 2004). One common conclusion of all these studies is that in the year with anomaly large snow cover over the TP, the Asian summer monsoon precipitation in the subsequent summer is anomalously high over the YR and is anomalously low over the SC. On the other hand, in the year with anomalously low snow cover over the TP, a reverse pattern can usually be observed.

The increase in soil moisture due to snow-melt could be an important factor for this change in the precipitation pattern since its memory is relatively long. In this study, six numerical experiments with different initial soil moisture of 20 %, 30 %, 40 %, 50 %, 60 % and 70 % at TP were performed using a regional climate model (Chan et al. 2004) running for the period from 1 April to 30 June 1998. The control experiment is the one with the value of 30 %. The results of the experiments show that the initial soil moisture at TP (ISMTP) in the spring period has a relatively long memory for the local as well as regional climate. In particular, as shown in Figs. 1 and 2, the increase in the ISMTP could in general result in an increase in the amount of monsoon precipitation over YR, a decrease in the monsoon precipitation over SC, and a southward shift in the position of the Baiu rainband over Japan. These patterns of precipitation differences due to changes in ISMTP in the sensitivity experiments are consistent with the corresponding patterns due to anomalous snow covers over TP in winter or spring. The changes in the precipitation over SC and the Baiu rainband appear to be related to the meridional shift in the position of the Northwestern Pacific subtropical high in association with the changes in ISMTP. In addition to the changes in precipitation pattern, the local effects of the increase in the ISMTP could decrease the air temperature (Fig. 3), upward vertical velocity, evaporative fluxes, and surface heating over TP. Finally, It has also been shown in this study that the Tibetan High can be weakened for high ISMTP, and so the strength of the Asian summer monsoon

Reference

Chan, J. C. L., Y. Liu, K. C. Chow, Y. Ding, W. K. M. Lau and K. L. Chan, 2005: Design of a regional climate model for the simulation of south China summer monsoon rainfall. *J. Meteor. Soc. Japan* (in press)

Qian, Y. F., Y. Q. Zheng, Y. Zhang and M. Q. Miao, 2003: Responses of China's summer monsoon climate to snow anomaly over the Tibetan Plateau. *Int. J. Climatology*, **23**, 593-613.

Wu, T. W. and Z. A. Qian, 2003: The relationship between the Tibetan winter snow and the Asian summer monsoon and rainfall: an observational investigation. *J. Climate*, **16**, 2038-2051.

Zhang, Y., T. Li and B. Wang, 2004: Decadal change of the spring snow depth over the Tibetan Plateau: the associated circulation and influence on the east Asian summer monsoon. *J. Climate*, **17**, 2780-2793.

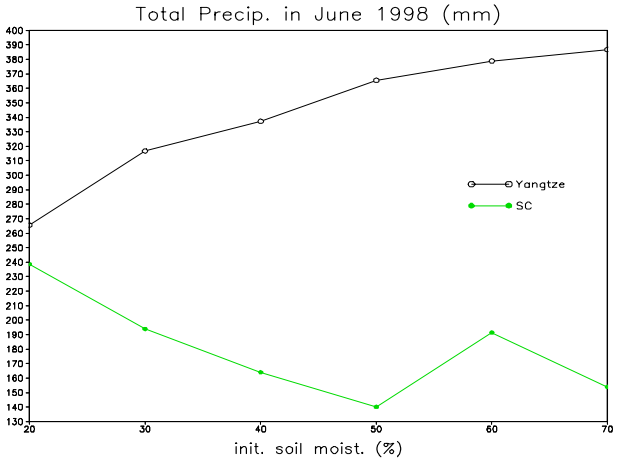

Fig. 1. Variation of total precipitation in June 1998 with different initial soil moisture at Tibetan Plateau over the Yangtze River region (28°-33°N, 115°-120°E) and the south China region (20°-27°N, 105°-120°E).

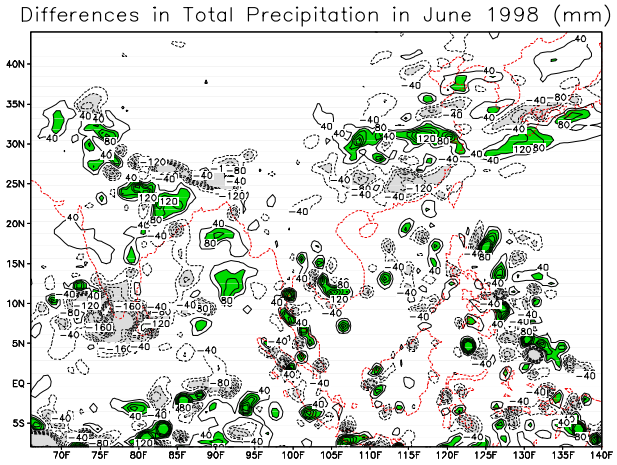

Fig. 2. Differences in total precipitation in June 1998 between the experiment with 70% initial soil moisture at Tibetan Plateau and the control experiment. Contour intervals are 40 mm with lighter shading denotes negative values less than -80 mm and darker shading for positive values greater than 80 mm.

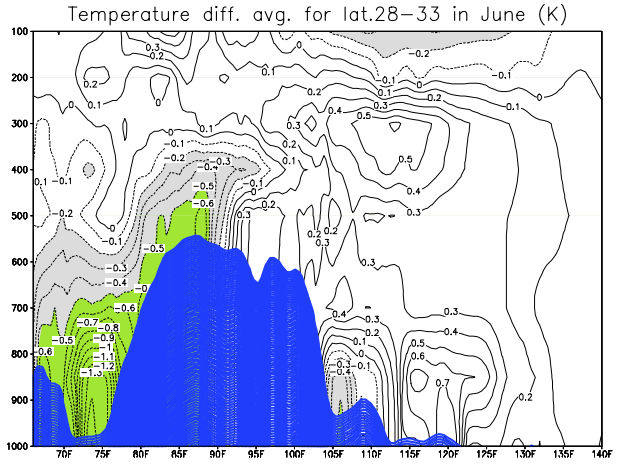

Fig. 3. Vertical profile of differences in temperature (K) averaged from 28° to 33°N. Contour intervals are 0.1 K and lighter shading denotes negative values less than -0.2 K and darker shading for negative values less than -0.6 K.

Current state of GEM climate simulation at RPN

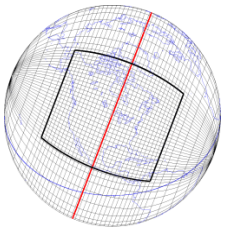

Bernard Dugas[1], Ayrton Zadra[1] and Katja Winger[2]

[1]Recherche en Prévision Numérique, Meteorological Service of Canada
[2]Université du Québec à Montréal
Bernard.Dugas@ec.gc.ca

1. Introduction

The Canadian Meteorological Centre/Recherche en Prévision Numérique (CMC/RPN) operational Global Environmental Multiscale (GEM) model is generally used to perform the short and medium range forecasts required by the Meteorological Service of Canada (MSC) clients. The model is also being used for seasonal forecasts, following its Historical Forecast (HFP) validation, and for even longer term type integrations. These last simulations and their comparison with climate means are essentially seen as a mean to evaluate the meteorological performance of the operational model. Accordingly, the recently developed Limited Area Model (LAM) GEM mode is a particularly important addition given the increasing resolutions at which even global operational forecast models are now routinely run.

2. Model and data

We compare results from a uniform 22-year AMIP2 (Atmospheric Model Intercomparison Project v2) simulation, from a 13-year SGMIP (Stretched Grid Model Intercomparison Project) variable resolution simulation and from a preliminary 2-year LAM (Limited Area Model) climate simulation, all using the GEM forecast model. These will be referred to by their acronyms in the following text. The AMIP2 also provides boundary conditions to the LAM. The same physics parameterizations are used for all three runs. The only differences relate to the horizontal grid used in each and the length of the time step. This is set at 22.5 minutes for SGMIP and LAM and 45 minutes for AMIP2. The LAM and SGMIP also share their maximum resolution area, which covers all of North America (NA) with a 50 km mesh. The number of horizontal mesh points on the SGMIP grid is approximately that of a global 1° uniform grid. The minimum SGMIP horizontal resolution is 1.8°, slightly less than the AMIP2 1.5° resolution. The vertical discretization is chosen such to be appropriate for the higher resolution SGMIP and LAM versions and consists of 60 hybrid vertical layers, with a top level at 2 hPa. The maximum vertical resolution occurs in the near the surface and in the PBL, with a 500 m secondary maximum around the equatorial tropopause. Results are compared with the freely available ERA40 reanalysis means for the corresponding periods.

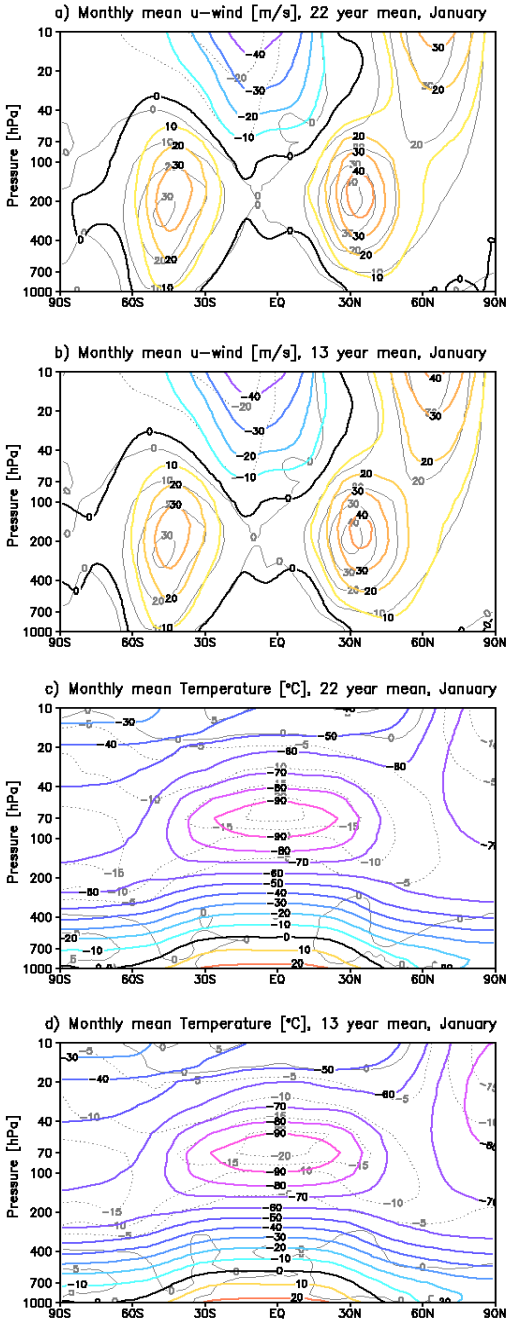

Fig. 1 January mean AMIP2 (a, c) and SGMIP (b,d)U and T. Pale lines indicate ERA40 U fields and T difference w.r.t. ERA40. Units are m/s and °C.

3. Results

The AMIP2 and SGMIP global means and variances are very similar and the only significant differences between them can be explained by the increased resolution over NA. The simulations display the same strength and weaknesses, *i.e.* a too deep troposphere which can be seen by the vertical displacement of both the mid-latitude zonal wind jets and of the Tropical tropopause.

AMIP2 and SGMIP suffer from excess precipitation over the mid-latitudes while there is a deficit over the ITCZ. This has been traced to the Kuo-type convection scheme and a correction is forthcoming. The deep troposphere is thought to be related to faulty radiation and cloud interaction in the tropics: As a consequence a more recent radiation code is also being implemented. SGMIP does manage to be in better balance than AMIP2 in terms of global energy and moisture budgets. With respect to the transient evolution of these budget terms, SGMIP is generally closer to ERA40 than is AMIP2.

Finally turning to the high resolution domain results, Fig. 2 shows the January mean surface air temperatures over most of NA for AMIP2, SGMIP and LAM, respectively. All three images are very similar, except that, as expected, the LAM and SGMIP show much more detail, particularly over the Western part of the continent where the orography is important. At this point, we believe that most of the differences between the LAM and SGMIP results can be explained by the different averaging periods. Further tests where the LAM is driven by a SGMIP-configured model are currently under way to verify this.

4. Conclusions

The results from the AMIP2 and SGMIP simulations are very similar with respect to the large scales. The two generally share the same strengths and weaknesses. As expected, significant differences between the two can be seen over the SGMIP North-American high resolution domain.

The SGMIP and LAM results over North America are also rather similar. Some of the differences can probably be attributed to the small number of samples in this preliminary LAM simulation.

Acknowledgements

The authors gratefully acknowledge the help of Michel Desgagné and Lubos Spacek, both of RPN, with the GEM/LAM version. This research was partly supported by CFCAS through a grant to the Regional Climate Network and by the Office of Science (BER), U.S. Department of Energy, Grant No. DE-FG02-01ER63199.

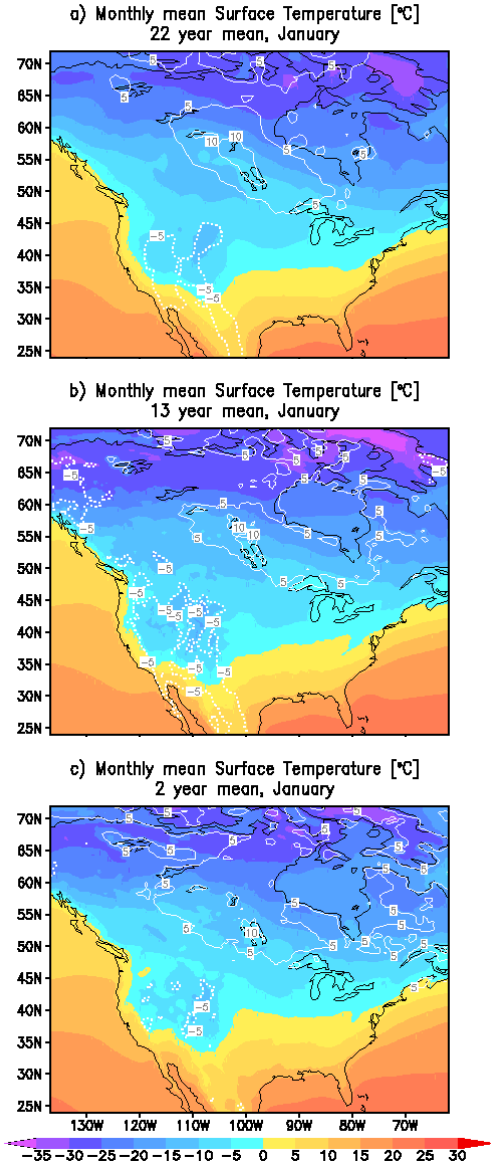

Fig. 2 January mean AMIP2 (a), SGMIP (b) and LAM (c) surface air temperatures. White lines indicate difference w.r.t. ERA40. Units are in °C.

References

Côté, J., S. Gravel, A. Méthot, A. Patoine, M. Roch and A. Staniforth (1998). The operational CMC-MRB Global Environmental Multiscale (GEM) model. Part I: Design considerations and formulation. *Mon. Wea. Rev.*, **126**, pp. 1373-1395.

Côté, J., J.-G. Desmarais, S. Gravel, A. Méthot, A. Patoine, M. Roch and A. Staniforth (1998). The operational CMC-MRB Global Environmental Multiscale (GEM) model. Part II: Results. *Mon. Wea. Rev.*, **126**, pp. 1397-1418.

European discharge under climate change conditions simulated by a multi-model ensemble

Stefan Hagemann and Daniela Jacob

Max Planck Institute for Meteorology, Bundesstr.53, 20146 Hamburg, Germany
Email: Hagemann@dkrz.de, Jacob@dkrz.de

Ten regional climate models (RCMs) participated in the European project PRUDENCE (Prediction of Regional scenarios and Uncertainties for Defining EuropeaN Climate change risks and Effects; http://prudence.dmi.dk/index.html), which aim was to predict uncertainties in RCM simulations over Europe (Christensen et al., 2005). Within PRUDENCE two major climate simulations were performed by each participating RCM. A control simulation representing current climate conditions for the period 1961-1990, and a scenario simulation representing climate change conditions according to the IPCC scenario A2 for the period 2071-2100. Lateral boundary conditions were provided by the atmospheric general circulation model (GCM) HadAM3H (Pope et al., 2000) for both simulations. In order to perform hydrological studies on these RCM simulations, a special focus was put on the discharge from large river catchments located in northern and central Europe. The discharge was simulated with a simplified land surface (SL) scheme (Hagemann and Dümenil Gates, 2003) and the Hydrological Discharge (HD) model (Hagemann and Dümenil Gates, 2001). The daily fields of precipitation, 2m temperature and evapotranspiration from the RCM simulations were used as forcing. Therefore the total catchment water balances are constrained by the hydrological cycle of the different RCMs.

The validation of the simulated hydrological cycle in the current climate has shown that a large spread exists between the models, but that the multi-model ensemble mean can be used to reduce uncertainty introduced by the use of a single RCM. This reduction can be achieved since the multi-model ensemble mean is usually closer to the observations than each of the models, especially if several catchments and hydrological variables are considered. Significant deviations of the ensemble mean to the observations point to common model problems, such as the prominent summer drying problem over Central Europe (Hagemann et al., 2004). Despite of the large differences in the control simulations of the RCMs, where the performance of the RCMs is different over the diverse catchments, the A2 climate change signal is very much confined and similar for almost all of the models. And even those RCMs who particularly disagree with regard to P and E in the control simulations, the A2 signal in the discharge is largely constrained by each of the models. This provides some confidence in the future projections even if only a few of the 10 RCMs may be considered. The results also indicate that the changes over the maritime Baltic Sea catchment are mainly related to changes in the large-scale circulation, while over the more continental Danube catchment the effect of local scale processes seems to be more important.

The following changes are predicted by the multi-model ensemble mean. For the Baltic Sea catchment, the precipitation will increase in the winter half of the year (October-March), and evapotranspiration will increase during the whole year with a maximum increase in the winter. These rises in precipitation and evapotranspiration will lead to an increase in discharge (>20%) only in the winter and early spring (Fig. 1). For the Danube, the precipitation will increase in the late winter (January-March) and decrease in the summer. The evapotranspiration will rise during the whole year, except for the summer, with a maximum increase in the winter. In the summer, a decrease is predicted. These changes lead to a large reduction (>20%) in the discharge throughout the year except in the late winter (Fig. 2). Here increases of about 10% are predicted. It seems that the large summer warming intensifies the drying of the Central European area represented by the Danube catchment. These results show that a strong gradient in the climate change signal is predicted by the RCMs. The future warming is intensifying the hydrological cycle in the north of Europe while over Central Europe the warming causes a weakening.

During the summer, the predicted changes by the GCM HadAM3H and the RCM HadRM3P deviate significantly from the RCM multi-model ensemble mean, especially for temperature, precipitation and evapotranspiration. As this common model behavior of the HadM3 model family seems to be independent of resolution, it is probably related to problems in representing certain local effects that are simulated differently than by the other RCMs. Despite of these problems of the driving GCM, almost all RCMs predict consistent changes in the hydrological cycle for all catchments. This indicates that the use of RCMs can compensate problems that a driving GCM might have with the

representation of local scale processes or parameterizations. Thus, in addition to the higher resolution, a further added value is obtained by the use of the RCM multi-model ensemble mean compared to the GCM.

It has to be noted that in this study only one scenario was considered, and only forcing from one GCM simulation was used. Results of Déqué et al. (2005) indicated that regarding uncertainty based on several models, the number of GCM forcings involved is at least as important as the number of RCMs, and that it is also necessary to consider several scenarios in the case of southern Europe summer warming. How RCM predictions behave using different scenarios and different GCM forcing will be investigated within the forthcoming European Union project ENSEMBLES that started in September 2004. First results considering two different scenarios and two different GCM forcings were obtained with RCAO (Räisänen et al., 2004) within the PRUDENCE project. Here, the four simulations agree on a general increase in precipitation in northern Europe especially in winter and on a general decrease in precipitation in southern and central Europe in summer, but the magnitude and the geographical patterns of the change differ markedly between the two GCM forcings.

References

Christensen, J.H., Christensen, O.B., and al.: 2005, 'PRUDENCE special issue introduction paper (title and co-authors to be finalized)', *Climatic Change*, submitted.

Déqué, M., Rowell, D., Schär, C., Giorgi, F., Christensen, J. H., Rockel, B., Jacob, D., Kjellstrom, E., de Castro, M., and van den Hurk, B.: 2005, 'An intercomparison of regional climate models for Europe: assessing uncertainties in model projections', *Climatic Change*, submitted.

Hagemann, S. and Dümenil Gates, L.: 2001, 'Validation of the hydrological cycle of ECMWF and NCEP reanalyses using the MPI hydrological discharge model', *J Geophys Res* **106**, 1503-1510.

Hagemann, S. and Dümenil Gates, L.: 2003, 'Improving a subgrid runoff parameterization scheme for climate models by the use of high resolution data derived from satellite observations', *Clim. Dyn.* **21**, 349-359.

Hagemann, S., Machenhauer, B., Jones, R., Christensen, O.B., Déqué, M., Jacob, D., and Vidale, P.L.: 2004, 'Evaluation of Water and Energy Budgets in Regional Climate Models Applied Over Europe', *Clim. Dyn.* **23**, 547-567.

Pope, V.D., Gallani, M.L., Rowntree, P.R., and Stratton, R.A.: 2000, 'The impact of new physical parametrizations in the Hadley Centre climate model: HadAM3', *Clim Dyn* **16**, 123-146.

Räisänen .J, Hansson, U., Ullerstig, A., Döscher, R., Graham, L.P., Jones, C., Meier, H.E.M., Samuelsson, P., and Willén, U.: 2004, 'European climate in the late twenty-first century: regional simulations with two driving global models and two forcing scenarios', *Clim. Dyn.* **22**, 13-31.

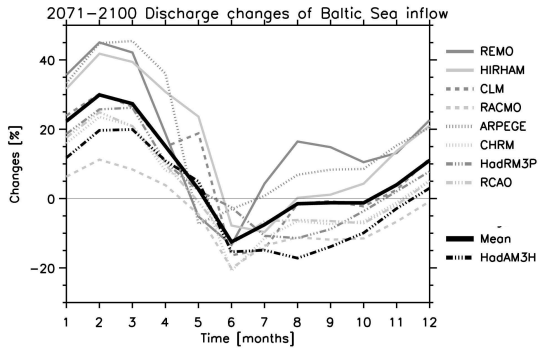

Figure 1 Mean monthly discharge Baltic Sea catchment. Mean designates the multi-model ensemble mean change of 8 RCMs (The other 2 RCMs did not cover the whole area).

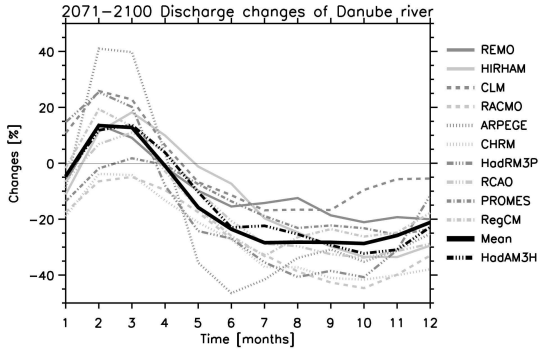

Figure 2 Mean monthly discharge changes in the Danube catchment. Mean designates the multi-model ensemble mean change of the 10 RCMs.

Influence of a New Stochastic Physics Scheme on Weather Regimes in the North Pacific Region

T. Jung[1], T.N. Palmer[1], and G.J. Shutts[1,2]
[1] ECMWF, Shinfield Park, Reading, RG2 9AX, United Kingdom
[2] MetOffice, Exeter, United Kingdom

Improvements of atmospheric circulation models in recent years have led to a substantial reduction of systematic model error in the short-range and medium-range; in the extended-range and beyond, however, systematic errors still constitute a significant source of forecast uncertainty (Jung, 2005). Moreover, the spatial structure of systematic model error has hardly changed during the last two decades (in the ECMWF model). As pointed out by Palmer (2001), one way to explain the above characteristics is that the very methodology used to approximate the equations of motion (i.e., neglecting the variability of unresolved scales) is itself a source of large-scale systematic error. From the above reasoning Palmer (2001) proposes the use of stochastic-dynamical parameterization schemes.

Such a scheme, which is based on a combination of a cellular automaton model (CA) with a stochastic backscatter scheme (SB), has recently been developed at ECMWF (Shutts 2004, Palmer et al. 2005). In this new stochastic physics scheme (CASB hereafter), the pattern of the stream function perturbation matches that of the CA and its (local) magntiude is proportional to the square root of the dissipation rate associated with the conventional parametrizations.

In this study we describe first results from climate runs with the ECMWF model without (CNTL hereafter) and with (CASB hereafter) the new stochastic physics scheme. The focus is on systematic error of the atmospheric circulation in the North Pacific region interpreted in terms of the frequency of occurrence of weather regimes. The model cycle used (26r3) has been operational at ECMWF from 7 October 2003 to 8 March 2004. The resolution used is T_L95 with 60 levels in the vertical. For each winter of the years 1962–2001 one 6-month long integration has been carried out (started at 1 October). The focus of this study is on the North Pacific region and the winter months from December through March. ERA-40 data are used for verification. The main parameter being considered is geopotential height at the 500hPa level (Z500).

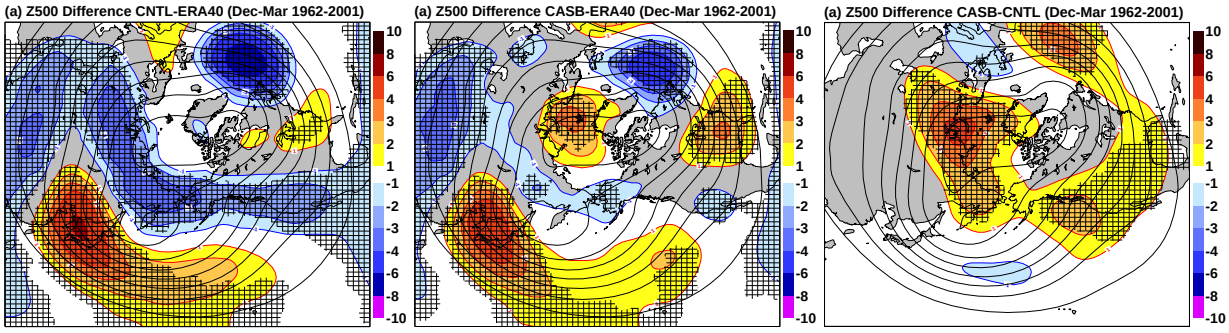

Figure 1: Difference of wintertime (Dec–Mar) mean Z500 (*dam*) between (a) the control integration and ERA-40 data, (b) the integration with the new stochastic physics scheme and ERA-40 data, and (c) the integration with the new stochastic physics scheme and the control integration. Results are based on 40 seasonal integrations (1962–2001) with the ECMWF model. Statistically significant differences (at the 95% confidence level) are hatched.

Systematic Z500 errors for the control integration are shown in Fig. 1a. In the North Pacific the model clearly overestimates the strength of the mid-latitude westerly winds. This overestimation is considerably reduced in the experiment with the CASB scheme (Fig. 1b). The Z500 difference between CASB and CNTL is shown in Fig. 1c and confirms that the CASB scheme has a significant impact on the model climate in the extratropics. It is worth mentioning, that the reduction of the westerly wind bias by the CASB scheme is consistent with a significant improvement of the frequency of occurrence of North Pacific blocking events described by Palmer et al. (1995).

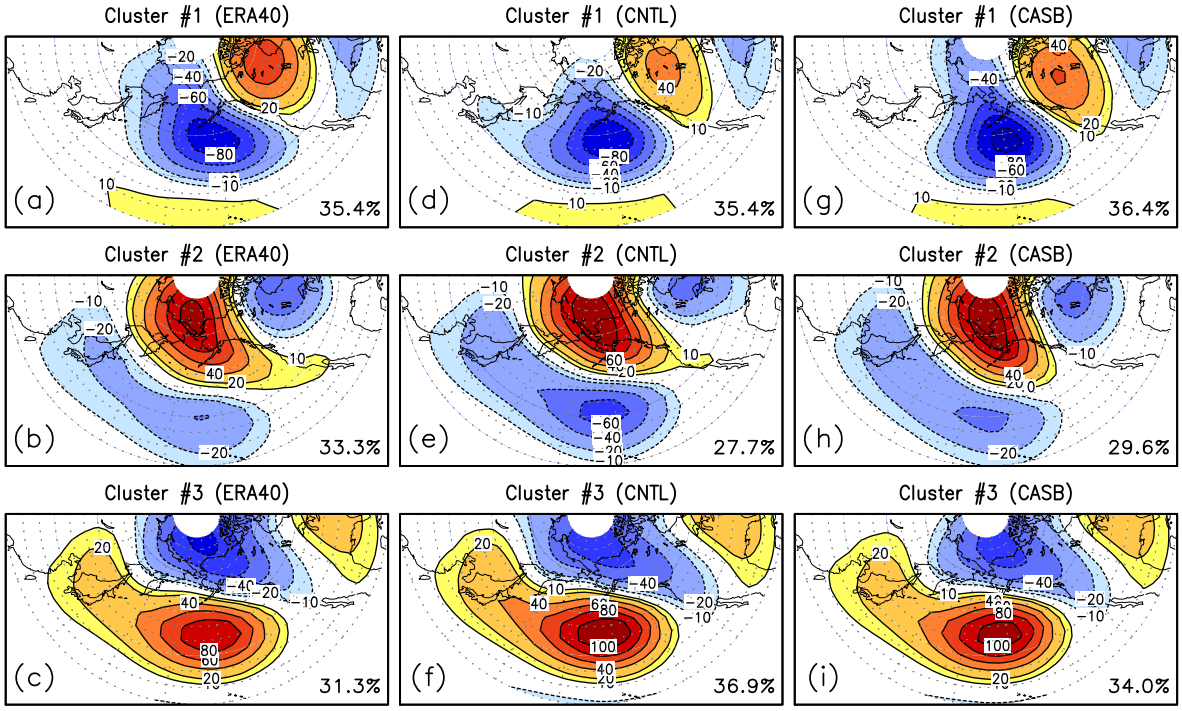

Figure 2: The first three clusters of wintertime Z500 anomalies (m): (a)–(c) ERA-40 reanalysis data, (d)–(f) control integration, and (g)–(i) integration with the new stochastic physics scheme (CASB). The results are based on 40 seasonal integrations (1962–2001) of the ECMWF model (cycle 26r3). The percentage of days spent in each of the clusters is also given.

In order to study simulated weather regimes in the North Pacific, K-means cluster analysis has been carried out. The analysis has been applied to the ten leading PCs of lowpass-filtered Z500 anomalies (annual cycle has been removed). The resulting three Z500 clusters are shown in Fig. 2 for ERA-40 data (left panel), the control integration (middle panel), and the experiment with the CASB scheme (right panel). The first thing to notice is that the ECMWF model, both, with and without stochastic physics, performs extremely well in simulating the spatial structure of the three observed cluster centroids. (Note, that separate analyses have been carried out for each of the datasets.) Furthermore, the frequency of occurrence of the first cluster is also very well simulated by the ECMWF model. The frequency of occurrence of the second and third cluster, however, is underestimated and overestimated, respectively, by the model compared to the observations. This frequency bias is consistent with a mean westerly wind bias shown in Fig. 1. Interestingly, the underestimation (overestimation) of the frequency of occurrence of the second (third) cluster is reduced in the experiment with the CASB scheme. Summarizing, the model error in simulating the frequency of occurrence of weather regimes has been almost halved by the introduction of the CASB scheme. For a more detailed discussion of how the CASB scheme might have changed the large-scale circulation the reader is referred to the papers by Palmer (2001) and Palmer et al. (2005).

References

Jung, T., 2005: Systematic errors of the atmospheric circulation in the ECMWF forecasting system. *Quart. J. Roy. Meteor. Soc.*, in press.

Palmer, T.N., 2001: A nonlinear dynamical perspective on model error: A proposal for non-local stochastic-dynamic parameterization in weather and climate prediction models. *Quart. J. Roy. Meteor. Soc.*, **127**, 279–304.

Palmer, T.N., G.J. Shutts, R. Hagedorn, F.J. Doblas-Reyes, T. Jung, and M. Leutbecher, 2005: Representing model uncertainty in weather and climate prediction. *Ann. Rev. Earth Planet. Sci.*, in press.

Shutts, G.J., 2004: A stochastic kinetic energy backscatter algorithm for use in ensemble prediction systems. *ECMWF Tech. Mem. 449.*

Contribution of natural and anthropogenic causes in regions with large temperature changes during XX century

Karpenko A.A.[1], Mokhov I.I.[1], Stott P.A.[2]

[1] A.M. Obukhov Institute of Atmospheric Physics RAS, Moscow, Russia
[2] Met Office, Hadley Centre for Climate Prediction and Research, UK

Global annual-mean surface air temperature (SAT) has been increasing during last three decades of 20th century at about 0.2 K/decade (Stott et al., 2000). Comparisons of observations with the climate model simulations show that both natural and anthropogenic factors have contributed significantly to 20th century temperature changes. According to model simulations the global warming during last decades cannot be explained by natural externally forced or internal variability (Stott et al., 2000; Climate Change 2001; Stott, 2003).

Maximum values of regional SAT trends during last decades are several times larger than that for global-scale SAT (Stott et al., 2000). Figure 1 shows an example of the annual-mean SAT trends from observations (RIHMI data - see (Razuvaev et al., 1993)) over the 30-year running intervals for Irkutsk (52N,104E) in Siberia. During last three decades of 20th century the SAT trend in this region was larger than 0.8 K/decade. Similar trends about 0.8 K/decade have been noted in the Northern Hemisphere during last decades at other Siberian sites and in Alaska. The largest SAT trend in the Southern Hemisphere was noted for the Antarctic Peninsula (up to 0.5 K/decade).

Figure 1 shows the annual-mean SAT trends and corresponding coefficients of correlation r over the 30-year running intervals from observations and HadCM3 simulations (ensemble of four model runs and ensemble mean) for region near Irkutsk with natural, anthropogenic and all forcings (see (Tett et al., 2002; Stott, 2003)). According to Fig.1 local SAT trends from observations at some sites are even larger than simulated regional (over model grid) trends for last decades of 20th century. This difference can be related partly with a general underestimation of regional Siberian warming due to both anthropogenic and natural forcings during last three decades. In particular, analysis of Stott (2003) indicates that HadCM3 appears to overestimate aerosol cooling in Asia. It can be also important the difference between local (observations) and regional (over model grid 2.5^{o}x3.75^{o}) trends.

The corresponding analysis for region in Alaska (for instance, about 60-65N, 135-140W) also shows a larger positive trend during last three decades from observations (CRUTEM2(v) - see (Jones and Moberg, 2003)) in comparison with model simulations except one model run. Analysis for Antarctic Peninsula shows less statistically significant trend of SAT during last decades than that for Siberia and Alaska both from observations and model simulations. The SAT trend in Antarctic Peninsula for last decades from observations (in particular, for Bellingshausen station about 62S, 59W) is found in the range of model estimates from different numerical runs.

This work has been partly supported by the RFBR and RAS Program.

References

Climate Change 2001: The Scientific Basis. Intergovernmental Panel on Climate Change. J.T. Houghton, Y. Ding, D.J. Griggs et al. (eds.). Cambridge Univ. Press. Cambridge, 2001. 881 pp.

Jones, P.D., and A. Moberg (2003) Hemispheric and large-scale surface air temperature variations: An extensive revision and an update to 2001. *J. Climate*, **16**, 206-223.

Razuvayev V.N., Apasova E.G., Martuganov R.A., Steurer P., Vose R., 1993. Daily Temperature and Precipitation Data for 223 U.S.S.R. Stations. ORNL/CDIAC, Numerical Data Package – 040, Oak Ridge Nat. Lab., Oak Ridge, Tennessee, USA.

Stott, P.A., S.F.B. Tett, G.S. Jones, M.R. Allen, J.F.B. Mitchell, and G.J. Jenkins (2000) External control of 20th century temperature by natural and anthropogenic forcings. *Science*, **290**, 2133-2137.

Stott, P.A. (2003) Attribution of regional-scale temperature changes to anthropogenic and natural causes. *Geophys. Res. Lett.*, **30**, 1728, doi:10.1029/2003GL017324.

Tett, S.F.B., et al. (2002) Estimation of natural and anthropogenic contributions to 20th century temperature change. J. *Geophys. Res.*, **107**, doi:10.1029/2000JD000028.

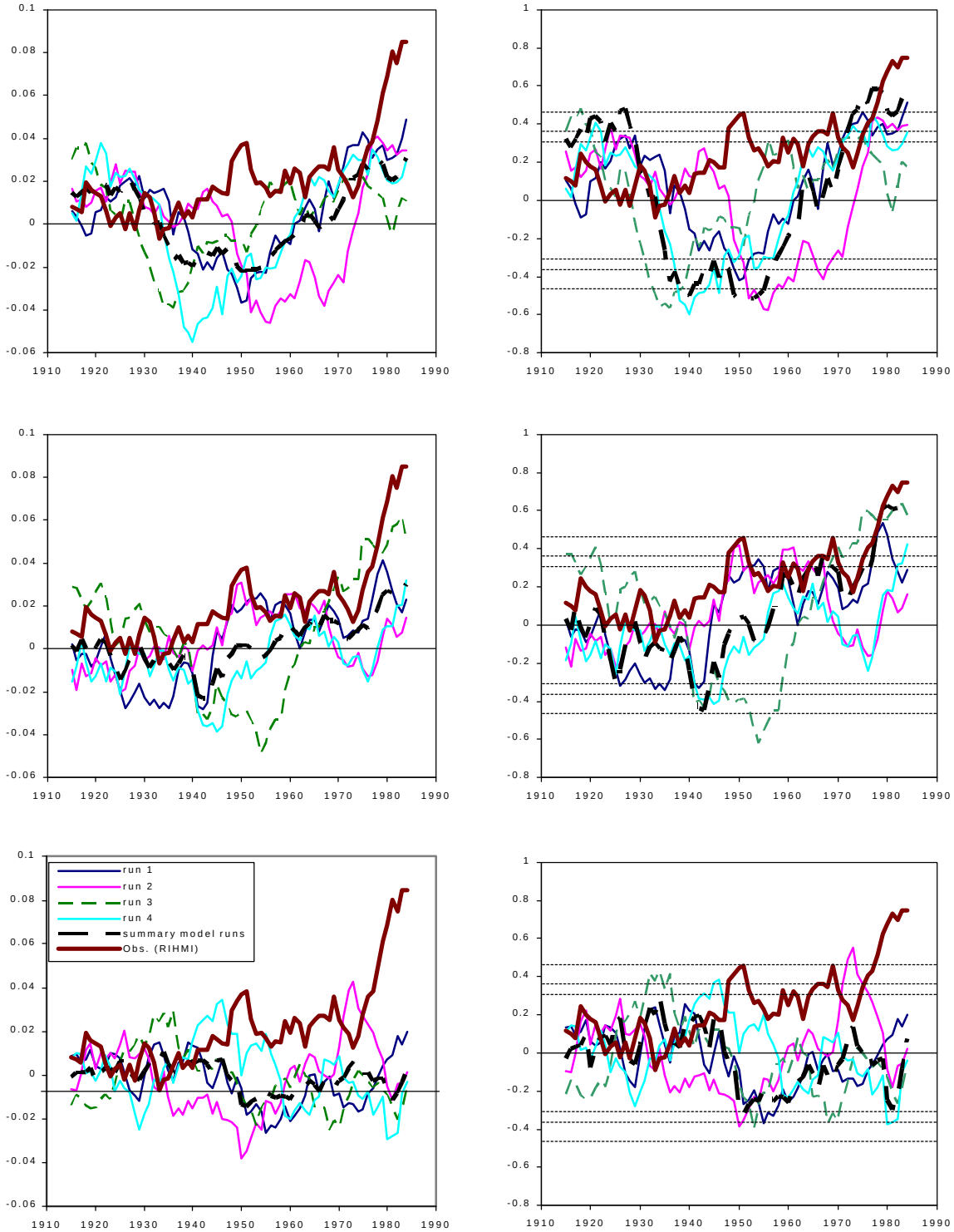

Fig.1. The annual-mean SAT trends (K/year, left panels) and corresponding coefficients of correlation r (right panels) from observations and model simulations over the 30-year running intervals for region near Irkutsk: all forcings (top panels), anthropogenic forcing (middle panels) and natural forcing (bottom panels). Dotted lines show minimum values of r for statistical significance of trends at the 90%, 95% and 99% level. The 30 year trends are centred on the year marked on the horizontal axis.

Climate Simulations of the Barents Sea Region

Elke Keup-Thiel, Tanja Blome and Daniela Jacob

Max-Planck-Institute for Meteorology, Bundesstrasse 53, D-20146 Hamburg,
email: keup@dkrz.de

In the context of the EU-Project BALANCE (http://balance1.uni-muenster.de) the regional climate model REMO is used for extensive calculations of the Barents Sea climate to investigate the vulnerability of the Barents Sea region to climate change. Together with fifteen participating institutes from Norway, Sweden, Netherlands, Finland, the United Kingdom and Germany the influence of climate change is studied for the Barents Sea region. This project addresses a large variety of Earth system components, including the terrestrial and the marine ecosystems as well as some of the economic sectors, such as fishery/aquaculture, forestry and reindeer husbandry.
To investigate the climate of the Barents Sea region (Figure 1) the following simulations have been performed with the hydrostatic regional climate model REMO (Jacob, 2001). For simulations of today's climate of the Barents Sea region REMO has been calculated from 1979 until 2000 at ~18 km horizontal resolution. For initialization and at the boundaries Analysis- and Reanalysis-data of the European Center for Medium range Weather Forecast (ECMWF) have been used. This simulation is called baseline run and has been validated with observations from the Arctic Meteorology and Climate Atlas (NSIDC, 2000). The validation has been focused on 2m-temperature and precipitation according to the available observations. The seasonal cycle of the 2m-temperature is relatively well simulated. However January and July seem to be 1-2 °C colder than the observations.

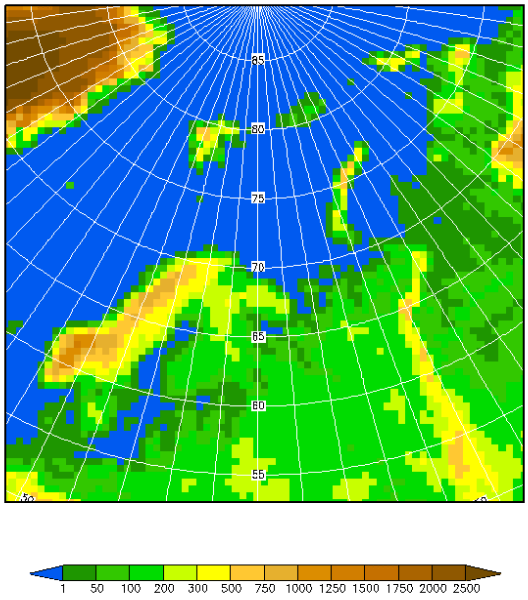

Figure 1: Model region of the Barents Sea, Orography [m].

A long run with the regional climate model REMO has been performed to simulate the climatic change of the Barents Sea region between 1961 and 2100 (Control and Climate Change run). For investigations of future climate development at ~50 km horizontal resolution REMO has been driven by the transient ECHAM4/OPYC3 IPCC-SRES B2 scenario (Roeckner, 1996). The ECHAM4/OPYC3 simulation has a warm bias in the sea surface temperature (SST), since it started 1860 using the SST of 1990. Therefore it is suggested (Roeckner et al., 1999) to look only at differences of time slices and not at the absolute values themselves. The analysis of the scenario describes the hypothetical changes in the Barents Sea region in the next century.

Decadal time slices have been investigated to point out in which season and in which region the biggest effects may occure. The annual mean 2m-temperature of the control and climate change run shows a clear trend as expected, the 2m-temperature increases about 5 degrees. The mean temperature over land is generally higher than the mean temperature over sea. The published temperature increase of the Arctic in the Arctic Climate Impact Assessment (ACIA, 2004) from 1960 to today of 1.5 ºC is in good agreement with our results. From 1960 to 2000 the annual mean temperature of the Barents Sea region rises exactly in the same way as in the simulation.

To investigate decadal changes four decades have been defined: a control period from 1980-1989, future decades from 2010-2019, 2040-2049 and 2070-2079. Only differences of these time slices will be analysed to point out where the biggest changes might be located. A stronger warming in January than in July is evident for all time slices. The warming is enhanced for the period 2040-2049 compared to the earlier period (2010-2019) as expected. The largest warming is located along the sea ice ridge and over Russia for the winter months.

References:

ACIA, 2004: Impacts of a warming arctic, http://amap.no/acia.

NSIDC, 2000: The Arctic Climatology Project – Arctic Meteorology and Climate Atlas. CD-Rome available by nsidc@kryos.colorado.edu, NSIDC, University of Colorado at Boulder.

Jacob, D. 2001: A note to the simulation of annual and inter-annual variability of water budget over the Baltic Sea drainage basin, Meteorology and Atmospheric Physics, Vol. 77, Issue 1-4, 61-73.

Roeckner, E., K. Arpe, L. Bengtsson, M. Christoph, M. Claussen, L. Duemenil, M. Esch, M. Giorgetta, U. Schlese, U. Schulzweida, 1996: The atmospheric general circulation model ECHAM4: Model description and simulation of present day climate Max-Planck-Institute for Meteorology, Report 218, 90p.

Roeckner, E., L. Bengtsson, J. Feichter, J. Lelieveld, and H. Rohde, 1999: Transient climate change simulations with a coupled Atmosphere-Ocean GCM including the tropospheric sulfur cycle, Journal of Climate, Vol. 12, 3004-3032.

Extreme Precipitation in Northern Eurasia from Observations and Model Simulations

V.Ch. Khon[1], I.I. Mokhov[1], E. Roeckner[2], V.A. Semenov[1,3]

[1]Obukhov Institute of Atmospheric Physics RAS, Moscow, Russia (khon@ifaran.ru)
[2]Max Planck Institute for Meteorology, Hamburg, Germany
[3]Institute for Marine Research at the University of Kiel, Germany

Characteristics of the daily precipitation (total precipitation, rain intensity, wet day probability and heavy precipitation) for different regions of Northern Eurasia in the XX-XXI centuries are investigated. Daily station data from the RIHMI (Razuvayev et al., 1993), gridded observational data from the CRU (New et al., 2000), data of the ERA-40 reanalysis (Simmons et al., 2000) and simulations with two generations of the global climate models ECHAM4/OPYC3 (Roeckner et al., 1996; Oberhuber, 1993) and ECHAM5/MPI-OM1 (Roeckner et al., 2003, Marsland et al., 2003) are analyzed (see also Semenov and Bengtsson, 2002, Voss et al., 2002, Mokhov et al., 2003, Mokhov et al., 2005).

In particular, estimates of the regional extreme precipitation changes have been made for basins of major Eurasian rivers, such as Volga, Ob, Yenisei and Lena rivers. A general increase of precipitation intensity is found for the all rivers basins from observations and simulations with ECHAM4/OPYC3 in the 20th century (Table1).

Table 1. Relative trends of precipitation intensity from the observational data CRU and simulations with ECHAM4/OPYC3 (1901-1996), %/100 years.

Basins	Winter	Summer	Annual	Winter	Summer	Annual
	CRU			ECHAM4/OPYC3		
Volga	1.6	4.4	3.1	3.1	2.3	5.3
Ob	4.4	2.1	2.9	0.1	8.0	5.0
Yenisei	6.2	0.1	1.8	4.4	7.0	5.1
Lena	8.7	3.5	3.4	6.3	3.8	4.5

According to observations the increase of precipitation intensity is the most significant for the Siberian rivers basins during wintertime of the 20th century (Table 1). Model results show significant enhancement of precipitation intensity and heavy precipitation (exceeding the 90% quantile) for the rivers basins during the 21st century (Fig.1, 2) with the most significant increase for the Siberian rivers basins in winter (Fig.1b, d). There are significant differences in tendencies of changes of wet day probability for the rivers basins during the 21st century: with a general increase in winter (Fig.1c) and a decrease in summer (Fig.2c).

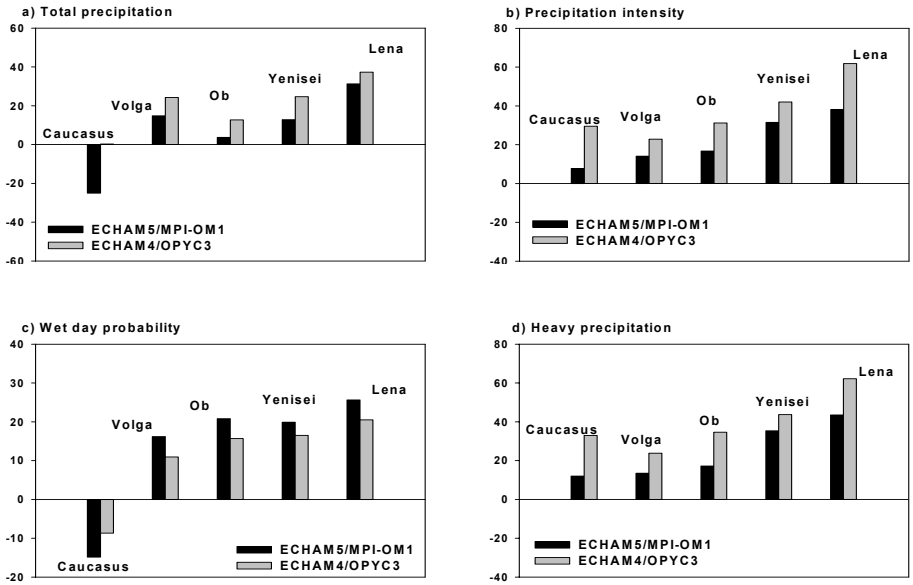

Figure 1. Relative trends for winter season: total precipitation (a), precipitation intensity (b), wet day probability (c) and upper 10% quantile (d) simulated by the ECHAM4/OPYC3 and ECHAM5/MPI-OM1 in the climate change experiment (1% greenhouse gases increase), %/100 years.

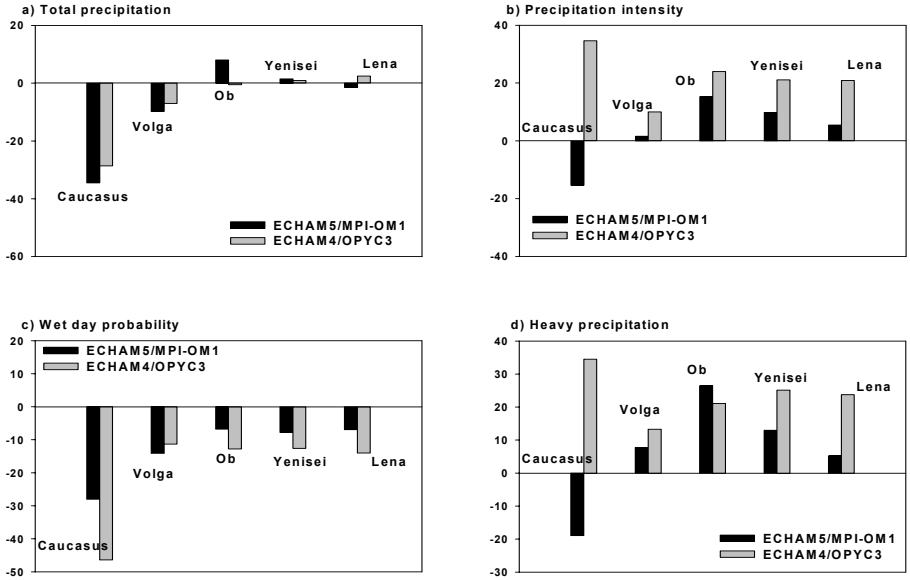

Figure 2. Same as in Figure 1 but for summer season.

Estimates of change of the extreme daily precipitation in Caucasian region from different data sets and models simulations are quite contradictory for summer season. For winter season model simulations show an increase of precipitation intensity (Fig.1b) and a decrease of wet day probability (Fig.1c) for Caucasian region during the 21st century.

In general, the model results show intensification of precipitation and its extreme values for the different regions of Northern Eurasia in the 21st century. According to observations and reanalysis the increase of the precipitation intensity already took place in the 20th century.

This work was supported by a NATO Collaborative Linkage project, RFBR and RAS program.

References

Marsland, S. J., H. Haak, J. H. Jungclaus, M. Latif, and F. Röske (2003): The Max-Planck-Institute global ocean/sea ice model with orthogonal curvilinear coordinates. Ocean Modell., 5, 91–127.

Mokhov, I.I., V.A. Semenov and V.Ch. Khon (2003): Estimates of Possible Regional Hydrologic Regime Changes in the 21st Century Based on Global Climate Models. Izvestiya, Atmospheric and Oceanic Physics, 39, 130–144.

Mokhov, I.I., E. Roeckner, V.A. Semenov and V.Ch. Khon (2005): Extreme regimes of precipitation in regions of Northern Eurasia in the 20th century and their possible changes in the 21st century. Doklady Earth Sciences (in press).

New, M., Hulme, M., Jones, P. (2000): Representing twentieth-century space-time climate variability. Part II: development of 1901–96 monthly grids of terrestrial surface climate. J. Climate. 13, 2217–2238.

Oberhuber, J.M. (1993): The OPYC Ocean General Circulation Model. Max-Planck-Institut fuer Meteorologie, Rep.7, 130 pp.

Razuvayev V.N., Apasova E.G., Martuganov R.A., Steurer P., Vose R. (1993): Daily Temperature and Precipitation Data for 223 U.S.S.R. Stations. ORNL/CDIAC, Numerical Data Package – 040, Oak Ridge Nat. Lab., Oak Ridge, Tennessee, USA.

Roeckner, E., Arpe, K., Bengtsson, L., Christoph, M., Claussen, M., Dümenil, L., Esch, M., Giorgetta, M., Schlese, U., Schulzweida, U. (1996): The atmospheric general circulation model ECHAM-4: model description and simulation of present-day climate. MPI Report 218, Max Planck Institute for Meteorology, Hamburg.

Roeckner, E., G. Bäuml, L. Bonaventura, R. Brokopf, M. Esch, M. Giorgetta, S. Hagemann, I. Kirchner, L. Kornblueh, E. Manzini, A. Rhodin, U. Schlese, U. Schulzweida, A. Tompkins (2003): The atmospheric general circulation model ECHAM 5. Part I: Model description. MPI Report 349, Max Planck Institute for Meteorology, Hamburg.

Semenov, V. and L. Bengtsson (2002): Secular trends in daily precipitation characteristics: greenhouse gas simulation with a coupled AOGCM. Climate Dynamics, 19, 123-140.

Simmons, A. J. and J. K. Gibson (2000): The ERA-40 Project Plan, ERA-40 Project Report Series No. 1, 63pp, ECMWF, Shinfield Park, Reading, UK.

Voss, R., May, W., Roeckner, E. (2002): Enhanced resolution modelling study on anthropogenic climate change: Changes in extremes of the hydrological cycle. Int. J. Climatol., 22 , 755-777.

Regional changes of Arctic sea ice and freshwater balance components from model simulations with anthropogenic forcing

V.Ch. Khon and I.I. Mokhov

Obukhov Institute of Atmospheric Physics RAS, Moscow, Russia (khon@ifaran.ru)

Arctic freshwater fluxes (such as Arctic sea ice export through Fram Strait and major Siberian rivers runoff) and their relationship to regional changes of sea ice, surface salinity and thermohaline circulation (THC) in the North Atlantic basin are analyzed using simulations of the coupled atmosphere-ocean general circulation model ECHAM4/OPYC3 (Roeckner et al., 1999) forced by the anthropogenic scenario IS92a.

Figure 1 shows time series of the annual mean export of Arctic sea ice through Frame Strait (a), sea ice concentration (a, b) and surface salinity (b) in the Greenland-Iceland-Norwegian (GIN) Sea basin for the period 1860-2100. According to the model simulations there is a statistically significant correlation between variations of Arctic sea ice flux through Frame Strait and anomalies of sea ice concentration in the GIN Sea (corresponding correlation coefficient r = 0.8). These changes of regional sea ice are negatively correlated (r = -0.9) to sea surface salinity in the GIN Sea (Fig. 1b).

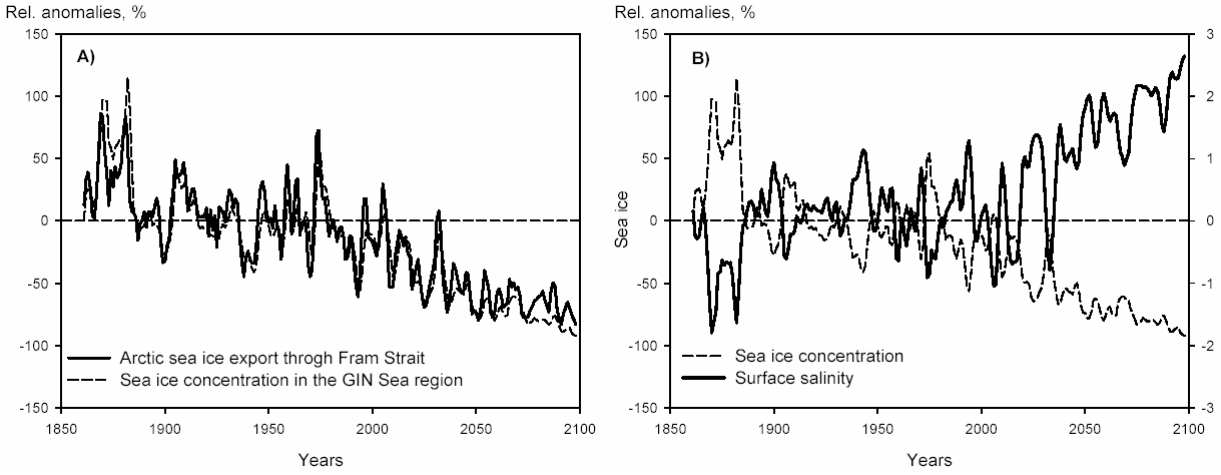

Figure 1. Annual mean anomalies (relative to 1961-1990) of the Arctic sea ice flux through Frame Strait and sea ice concentration in the GIN Sea (a); sea ice concentration and surface salinity in the GIN Sea (b) simulated by ECHAM4/OPYC3 (IS92a scenario) for the period 1860-2100.

Thus, the tendency of decrease of the Arctic sea ice flux through Fram Strait leads to significant positive anomaly of surface salinity in the GIN Sea basin in the 21st century. This effect is opposite to the "Great Salinity Anomaly" effect in the northern North Atlantic during the late 1960s (Dickson et al., 1982). The reduced sea ice export out of the Arctic basin induces anomalously high salinities in the North Atlantic basin and leads to an intensification of North Atlantic THC (Latif et al., 2000) during the 21st century. The correlation between salinity in the GIN Seas and the North Atlantic THC significantly increases in the 21st century (Table 1) with a maximum correlation coefficient at 0.67 when salinity leads THC by about 7 years.

Table 1. Maximum correlation coefficients (and corresponding time lags (years), in brackets) between Arctic sea ice volume flux through Frame Strait (IVF_FS) and sea surface salinity in the GIN Sea (SSS_GIN); between SSS_GIN and index of the North Atlantic thermohaline circulation (THC_NA).

	20th century	21st century
IVF_FS - SSS_GIN	-0.71 (1)	-0.83 (1)
SSS_GIN - THC_NA	0.27 (9)	0.67 (7)

Model simulations of sea ice dynamics and its connection with the large-scale atmospheric circulation is also investigated for winter season. Figure 2a shows correlation coefficients between wintertime-mean (December-March) index of Arctic Oscillation (AO index) and meridional drift of sea ice at Fram Strait for the 30-year running periods based on anthropogenic simulations with ECHAM4/OPYC3. According to Fig.2a the positive correlation between winter sea ice circulation and the AO index increases in the second half of the 20th century. This correlation becomes statistically significant at the confidence level > 90 % during winter of the 21st century. Figures 2b, c demonstrate anomalies of sea level pressure (SLP) associated with the AO index during the period of the anomalously low (b) and high (c) positive correlation between the AO index and meridional sea ice circulation. During phase of low correlation the AO-related SLP anomalies are mainly located in the northern North Atlantic basin (especially near Iceland) (Fig. 2b). The phase of high positive correlation (Fig. 2c) is characterized by anomalously low SLP in most eastern Arctic basin (Norwegian, Barents, Kara and Laptev Seas). This northeastward shift of the AO-related SLP anomalies (Fig.2c) leads to the pronounced anomalous southerly wind component between Greenland and Spitzbergen and, therefore, to the in-phase variability between the AO index and sea ice flux out of the Arctic basin.

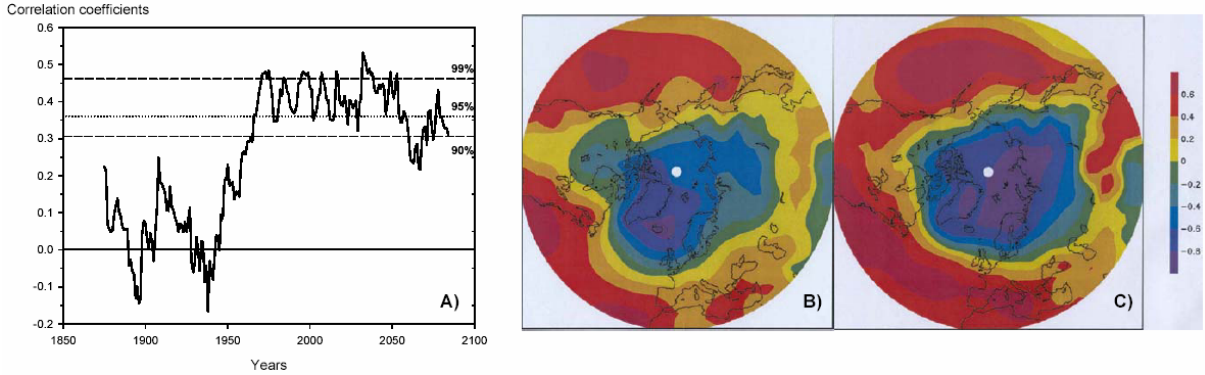

Figure 2. Correlation coefficients between AO index and meridional sea ice drift (a) for the 30-yr running periods; maps of correlation coefficients between winter AO index and SLP fields for selected periods of anomalously low (b) and high (c) correlations based on simulations with ECHAM4/OPYC3 (IS92a scenario).

Connection of major Siberian rivers (Ob, Yenisei and Lena) runoff (Mokhov et al., 2003) with the sea ice formation in the Kara and Laptev Seas is also investigated. Analysis of monthly observational data (Lammers et al., 2001; Rayner et al., 2003) shows that anomalies of sea ice in eastern Arctic basin (Kara and Laptev Seas) is positively correlated to variations of Siberian rivers runoff in the first months of cold season (especially in November) for the period 1935-1999. Analysis of ECHAM4/OPYC3 simulation indicates that model reproduces the positive correlation between regional sea ice and runoff of major Siberian rivers for the same period (and season) in the 20th century. Estimates of anthropogenic changes also demonstrate positive correlation of sea ice in Kara Sea with Ob and Yenisei runoff for the 21st century. According to model simulations the correlation between Lena runoff and sea ice in Laptev Sea becomes statistically insignificant in the 21st century.

References

Dickson, R.R., J. Meincke, S.-A. Malmberg, A.J. Lee, 1988: The ‘‘Great Salinity Anomaly’’ in the northern North Atlantic 1968– 1982. *Prog. Oceanogr.,* **20,** 103–151.

Lammers, R.B., A.I. Shiklomanov, C.J. Vorosmarty, B.M. Fekete, B.J. Peterson, 2001: Assessment of contemporary Arctic river runoff based on observational discharge records. *J. Geophys. Res.,* **106,** 3321-3334.

Latif, M., E. Roeckner, U. Mikolaewicz, and R. Voss, 2000: Tropical stabilization of the thermohaline circulation in a greenhouse warming simulation. *J. Climate,* **13,** 1809-1813.

Mokhov, I.I., V.A. Semenov, V.C. Khon, 2003: Estimates of possible regional hydrologic regime changes in the 21st century based on global climate models. *Izvestiya, Atmospheric and Oceanic Physics,* **39,** 130–144.

Rayner, N.A., D.E. Parker, E.B. Horton, C.K. Folland, L.V. Alexander, D.P. Rowell, E.C. Kent, A. Kaplan, 2003: Global analyses of sea surface temperature, sea ice, and night marine air temperature since the late nineteenth century. *J. Geophys. Res.,* **108,** 4407.

Roeckner, E., L. Bengtsson, J. Feichter, J. Lelieveld, and H. Rodhe, 1999: Transient climate change simulation with a coupled atmosphere-ocean GCM including the tropospheric sulfur cycle. *J. Climate,* **12,** 3004-3032.

Simulation of the surface climatology over the Eastern Mediterranean region using the RegCM3 model

Simon O. Krichak, Pinhas Alpert and Melina Dayan

Department of Geophysics and Planetary Sciences, Raymond and Beverly Sackler Faculty of Exact Sciences, Tel Aviv University, Tel Aviv, Israel
E-mails: shimon@cyclone.tau.ac.il, pinhas@cyclone.tau.ac.il, melina@cyclone.tau.ac.il

Results of regional climate of the Eastern Mediterranean region with third generation of the Regional Climate Model (RegCM3; Giorgi et al. 1999 and Pal et al. 2000) are evaluated through the comparisons with observed surface climatology. The dynamical core of the RegCM is essentially equivalent to the hydrostatic version of the NCAR/Penn State mesoscale model MM5. Surface processes are represented via the Biosphere-Atmosphere Transfer Scheme (BATS) and boundary layer physics is formulated following a non-local vertical diffusion scheme. Resolvable scale precipitation is represented via the scheme of Pal et al. (2000), which includes a prognostic equation for cloud water and allows for fractional grid box cloudiness, accretion and re-evaporation of falling precipitation. Convective precipitation is represented using a mass flux convective scheme while radiative transfer (Giorgi et al. 1999) is computed using the radiation package of the NCAR Community Climate Model, version CCM3. Cloud radiation is calculated in terms of cloud fractional cover and cloud water content, and a fraction of cloud ice is diagnosed by the scheme as a function of temperature. The model domain in the experiment (Figs. 1 - 3) covers the eastern Mediterranean region with a total of 45 x 34 Lamber Confomal grid points with 40 km horizontal resolution and 18 sigma levels in the vertical. The model is nested by the one-way relaxation Davies and Turner (1977) with the initial and lateral boundary conditions provided from NCEP/NCAR re-analysis project (NNRP) data (Kalnay et al. 1996) and the surface forcing is prescribed with observed weekly mean sea surface temperature Reynolds et al. (2002). The simulation was started on January 1, 1981 and was run continuously for 20 years with 3-minute time steps. The monthly and seasonal mean results from the model's simulation for five years from 1985 to 1989 are compared here with the observed screen surface temperature and precipitation from the Climate Research Unit (CRU; New et al. 2000), Climate Prediction Center global precipitation data (CPC; Xie and Arkin, 1996) and NNRP (Kalnay et al. 1996). The mean DJF precipitation simulated by the RegCM3 is consistent with Xie-Arkin observational data and describes the real precipitation space distribution with higher details than in the NNRP data. Most of the land precipitation produced by the RegCM3 is right concentrated in a very narrow band along the coastal zone. Fig. 2 shows the monthly mean surface temperature over the region. The agreement between RegCM3 simulation and CRU observation is quite good. The RegCM3 simulates accurately the seasonal variability of screen temperature over the main parts of the region. The research was supported by German-Israeli research grant (GLOWA - Jordan River) from the Israeli Ministry of Science and Technology; and the German Bundesministerium fuer Bildung und Forschung (BMBF).

References:

Davies, H. C. and Turner, R. (1977). Updating prediction models by dynamical relaxation: an examination of the technique. *Quart. J. of the Roy. Meteor. Soc.*
Giorgi, F., Y. Huang, K. Nishizawa and C. Fu (1999) A seasonal cycle simulation over eastern Asia and its sensitivity to radiative transfer and surface processes. *Journal of Geophysical Research*.
Pal, J.S., E.E. Small and E.A.B. Eltahir (2000) Simulation of regional-scale water and energy budgets: Representation of subgrid cloud and precipitation processes within RegCM. *Journal of Geophysical Research*.
Kalnay E, and coauthors (1996) The NCEP/NCAR 40-year reanalysis project, *Bull. Am. Met. Soc*.
New, M., M. Hulme, et al. (1999). Representing Twentieth-Century Space-Time Climate Variability. Part I: Development of 1961-90 Mean Monthly Terrestrial Climatology. Journal *of Climate.*
Reynolds, R.W., N.A. Rayner, T.M. Smith, D.C. Stokes, and W. Wang (2002) An Improved In Situ and Satellite SST Analysis for Climate, *J. Climate*.
Xie, P., and P. A. Arkin (1996). Analyses of global monthly precipitation using gauge observations, satellite estimates, and numerical model predictions. *Journal of Climate*.

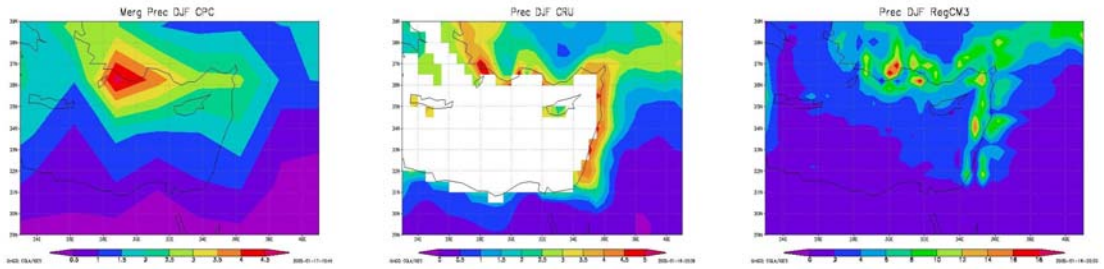

Figure 1. DJF Precipitation (mm/day)

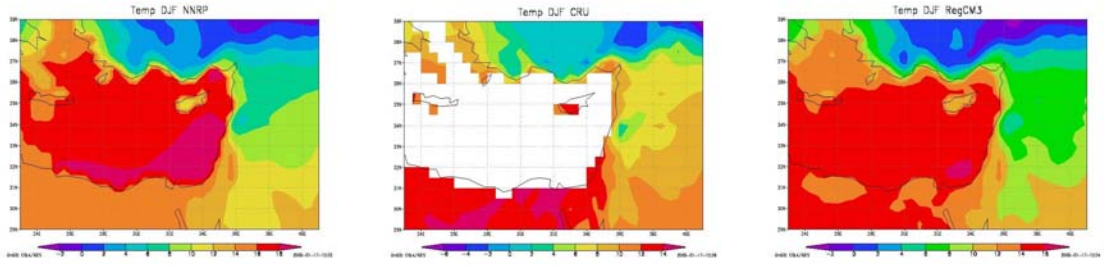

Figure 2. DJF Surface air temperature (°C)

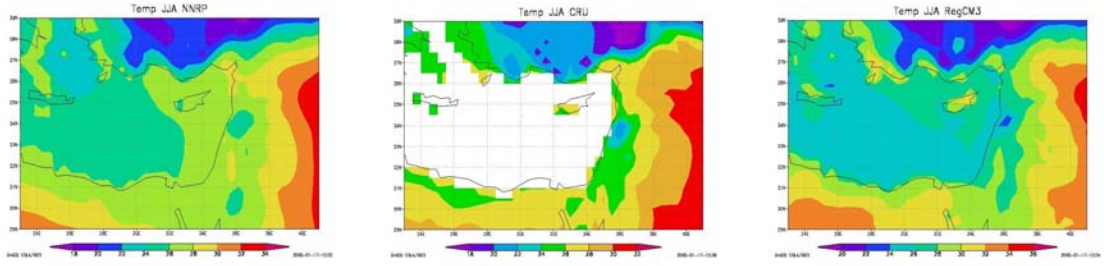

Figure 3. JJA Surface air temperature (°C)

Influence of regional scale information on the global circulation: A two-way nesting climate simulation

Philip Lorenz and Daniela Jacob

Max-Planck-Institute for Meteorology, Hamburg, Germany

philip.lorenz@dkrz.de

Introduction

A two way nested climate model system has been setup using a global and a regional atmospheric climate model. Within the domain of the regional model the global model is updated every timestep by the aggregated corresponding results of the regional model for this timestep. There is a feedback from the regional model to the global model.
A 10-year simulation has been carried out with this two way nested climate model system using a two way nested domain covering the equatorial Western Pacific region ("warm pool").

The two way coupled model system

To address a two-way-nesting (TWN) approach for coupling a regional atmospheric climate model with a global climate model, the Max Planck Institute for Meteorology (MPI-M) models REMO (Jacob, 2001) and ECHAM4 (Roeckner et al., 1996) were used. The ECHAM4 model is a global atmospheric general circulation model with a spectral representation of the prognostic variables except the water components. It is used in this work with a T42 horizontal resolution and a corresponding time step of 24 minutes.

Global Atmospheric Climate model ECHAM4		
•Resolution:	Horizontal: T42	Vertical: 19 Levels
•Time step:	24 minutes	
•Prognostic variables:		
Temperature		spectral
Divergence		spectral
Vorticity		spectral
spec. Humidity		grid
liquid water		grid
surface pressure		spectral
Regional Atmospheric Climate Model REMO		
•Resolution:	Horizontal: 1/2°	Vertical: 19 Levels
•Time step:	4 minutes	
•Prognostic variables:		
Temperature		grid
horizontal wind components (U,V)		grid
spec. Humidity		grid
liquid water		grid
surface pressure		grid

Table 1: Characteristics of the used models

REMO is a regional hydrostatic atmospheric climate model, the set of physical parameterizations of this model is absorbed from the global ECHAM4 model. It is used in this work with a 0.5° horizontal resolution with a corresponding time step of 4 minutes. The characteristics of the used models are shown in table 1.
In an (up to now used) one-way-nesting mode REMO is initialized and driven at the lateral boundaries using data from (Re)-Analysis products resp. global model output; there is no feedback from the regional model to the global model. Within the presented two-way-nesting approach, every time-step all the prognostic variables of the ECHAM4 model are updated within the regional model domain by the corresponding results of the REMO model for this time step. A schematic flow diagram of the two way nested system is shown in figure 1.

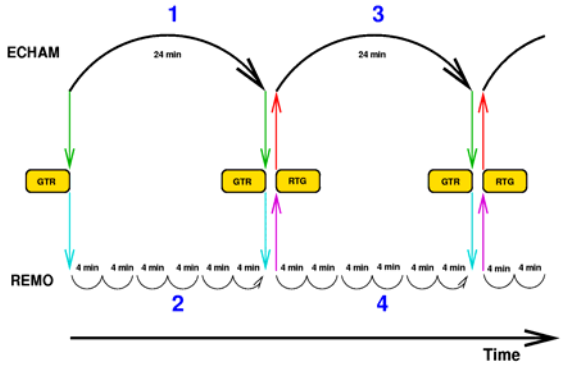

Fig. 1: Schematic flow diagram of the two way nested system. GTR: global to regional interpolation RTG: regional to global aggregation

Results of a 10 year Integration

A two-way-nested REMO-ECHAM4 run (ECHAM4(TWN)) and an ECHAM4 stand alone run (ECHAM4(ORI)), both initialized at the 1st of January 1980, were integrated for 10 years using observed SST data (AMIP); the two-way-nested regional domain covers the Western Pacific / Indonesian Warm Pool (110° E – 155° E; 12° S – 12° N; 91 x 49 grid points). Figure 2 shows the orography and land-sea-mask of the two-way-nested domain in the REMO 0.5°-horizontal resolution against the ECHAM4-T42 horizontal resolution.

The "warm pool" region has been chosen because it is an area with a very large energy input into the atmosphere. The poorly represented land-sea distribution and orography in the global model with the T42 horizontal resolution is much more realistic in the REMO 0.5° resolution.

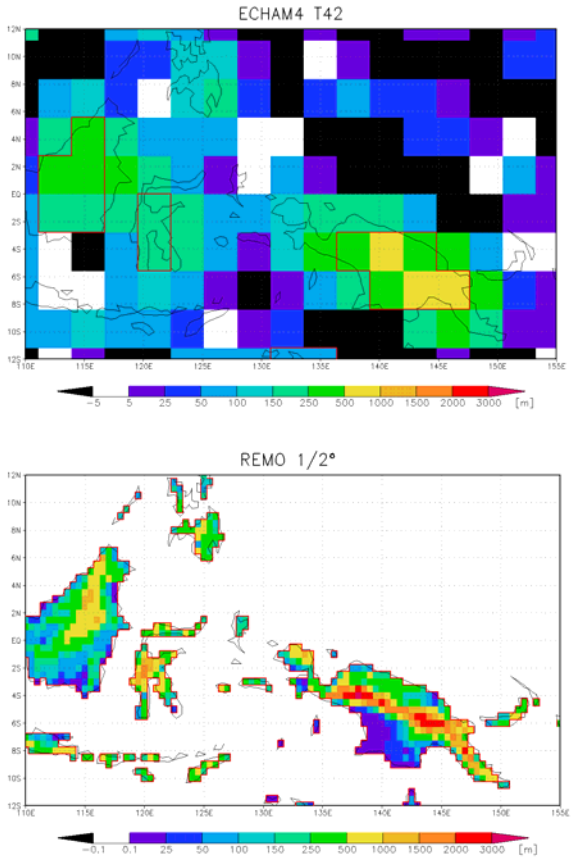

Fig. 2: Orography [m] and land-sea-mask (red line) of the two-way-nested region covering the Western Pacific "warm pool" region in the ECHAM4-T42 horizontal resolution (upper panel) and in the REMO 0.5° horizontal resolution (lower panel)

The comparison of the ECHAM4(ORI) run against the ERA 15 reanalysis data (figure 3; upper panel) shows the known systematic error of ECHAM4 (Roeckner et al., 1996): there is a significant cold bias in the polar upper troposphere and a warm bias of the tropical troposphere of the ECHAM4 model in T42 resolution. Figure 3 (lower panel) shows the influence of the two way nesting approach (ECHAM4(TWN) -ECHAM4(ORI): the relative warming of the polar upper troposphere and the cooling of the tropical troposphere indicates a reduction of the systematic temperature biases for the whole troposphere due to the two way nesting approach.

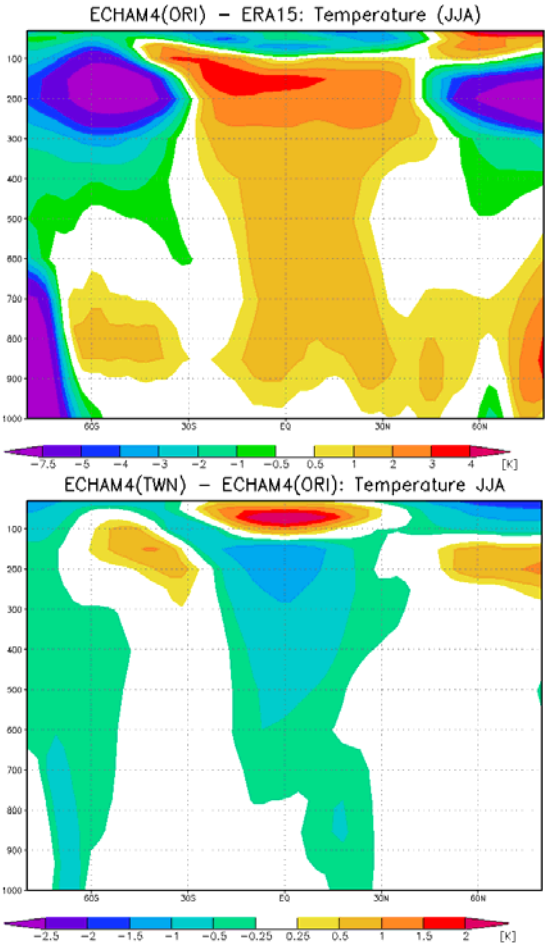

Fig. 3: 10 year seasonal (JJA) zonal mean temperature difference [K] ECHAM4(ORI) – ERA15 (upper panel) resp. ECHAM4(TWN) – ECHAM4(ORI) (lower panel).

Conclusions

The two way nested ECHAM4 – REMO atmospheric climate model system has been setup and can be integrated numerically stable for a 10-year period. Preliminary results show an influence on the simulated global climate, even in regions not covered by the two-way-nest domain. There are indications that the systematic error can be reduced by the finer resolution of specific regions that are important for the global circulation.

The results of the performed 10-year integrations will be analyzed in more detail.

References

Jacob, D., A note to the simulation of the annual and inter-annual variability of the water budget over the Baltic Sea drainage basin, Meteorology and Atmospheric Physics, Vol. 77, 61-73, 2001

Roeckner, E., K. Arpe, L. Bengtsson, M. Christoph, M. Claussen, L. Dümenil, M. Esch, M. Giorgetta, U. Schlese, U. Schulzweida: The Atmospheric General Circulation Model ECHAM-4: Model description and simulation of present-day-climate. Max Planck Institute for Meteorology, Hamburg, , Report No. 218, 1996

An assessment of the PRECIS Regional Climate Modelling System – Simulations over North America using PRECIS

Pascale Martineu
Canadian Regional Climate Modelling Network, UQAM,
UQÀM @ Ouranos, 550 Sherbrooke W., Montréal (Québec) H3A 1B9 Canada, martineu.pascale@uqam.ca

Introduction

PRECIS, Providing REgional Climates for Impacts Studies, is a regional climate modelling system developed by the Hadley Centre (Jones *et al*. 2003, Wilson *et al*. 2003). The PRECIS system is based on the latest RCM version developed at the Hadley Centre, and it has been designed to be user-friendly and easily implemented on any fast PC running a Linux system.

The PRECIS system has been tested over North America at the resolution of 0.44°, selecting different regions with different domain-sizes. The multi-years simulations of PRECIS were generated by applying lateral boundary conditions (dynamical atmospheric information) from ECMWF ReAnalysis data provided from 12/1978 to 05/1982. Seasonal means fields have been used for the different realizations.

Performances of PRECIS

a. Relative Speed of PRECIS

The monitoring of our PRECIS experiments identified a number of deficiencies. For example, the same CPU simultaneously runs the PRECIS simulation and PRECIS diagnostics, with at least 160 output variables of standard diagnostics. Consequently, the cocktail of diagnostics such as hourly mean/max/min surface and upper air, and daily mean/max/min surface and upper air diagnostics output in addition to standard climate meaning diagnostics is extremely demanding for the processor. As a result, the complete output diagnostic selection takes 15 times more time than other available selections (Fig. 1). Despite the sensitivity of the speed to diagnostic output selection and of course the domain size, the performance of the Intel Xeon 2.5Ghz Processor, i.e. our PRECIS environment, seems appropriate for PRECIS, faster than the standard Intel P4 processor.

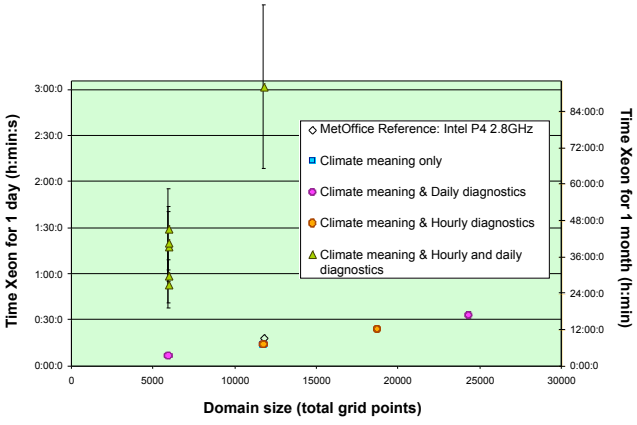

Fig. 1. Relative speed of Intel Xeon Processor 2.8Ghz running PRECIS related to diagnostic output selection and domain size.

b. Ability of PRECIS to simulate climate

CDAT (Climate Data Analysis Tools) is supplied with PRECIS to process the output data and visualize the results. Global datasets from the driving analyses (ERA) and observational datasets (CRU) are also supplied with PRECIS, i.e. global data as 3-month seasonal mean data for season (e.g. DJF: December to February, JJA: June to August) for the period from 12/1978 to 05/1982 (ERA dataset) or to 11/1982 (CRU dataset).

In order to evaluate our PRECIS experiments, these global data were regridded onto the three different grids used in our experimental setups: (A) Pan-Canada (180x135), Central-America and USA (135x110) and (C) eastern North America (79x75). Figures 2 and 3 show the comparison of 3-month seasonal mean data for winter and summer 1980 of PRECIS simulations at the resolution of 0.44° with ERA and CRU regridded datasets, i.e. the winter (DJF) and summer (JJA) mean Temperature at 1.5 m and Total Precipitation for the year 1980, after one-year (1979) spin-up. The added-value and the skill of PRECIS system, respectively 'PRECIS minus driving data' and 'PRECIS minus observational data', are also presented in Fig. 2 and 3.

Conclusion

Results obtained over the three different North American domains indicate a good ability of PRECIS at 0.44° to simulate the climate. The added-value of the high resolution is remarkable over topographic details such as the Rocky mountains, the Cordillera, the Arctic and Caribbean Islands. The general patterns of the screen temperature or the total precipitation are coherent with the observational datasets. Nevertheless, some differences do exist between PRECIS and the observations (e.g. seasonal CRU dataset). For example, PRECIS overestimates by 6°C the CRU temperature data over central USA for the summer 1980. But no conclusion can be made concerning the skill of PRECIS over Greenland or Canada/Arctic area because the observational data in this area are scattered and dubious quality.

References

Jones, R., D. Hassel, D. Hudson, S. Wilson, G. Jenkins and J. Mitchell, 2003. Workbook on generating high resolution climate change scenarios using PRECIS, ed. Met Office, UK, 32p.

Martineu, P. 2004: An assessment of the PRECIS Regional Climate Modelling System - Simulations over North America using PRECIS, *EOS Trans. AGU*, 85(47), Fall Meet. Suppl., A53A-0872

Mitchell, T.D., T.R. Carter, P.D. Jones, M. Hulme, and M. New, 2004. A comprehensive set of high-resolution grids of monthly climate for Europe and the globe: the observed record (1901-2000) and 16 scenarios (2001- 2100). *J. Clim.* (Subm.)

Wilson S., D. Hassel, D. Hein, R. Jones and R. Taylor, 2003. Installing and using the Hadley Centre regional modelling system - PRECIS version 1.0, ed. Met Office, UK, 108p.

PRECIS web site : http://www.precis.org.uk

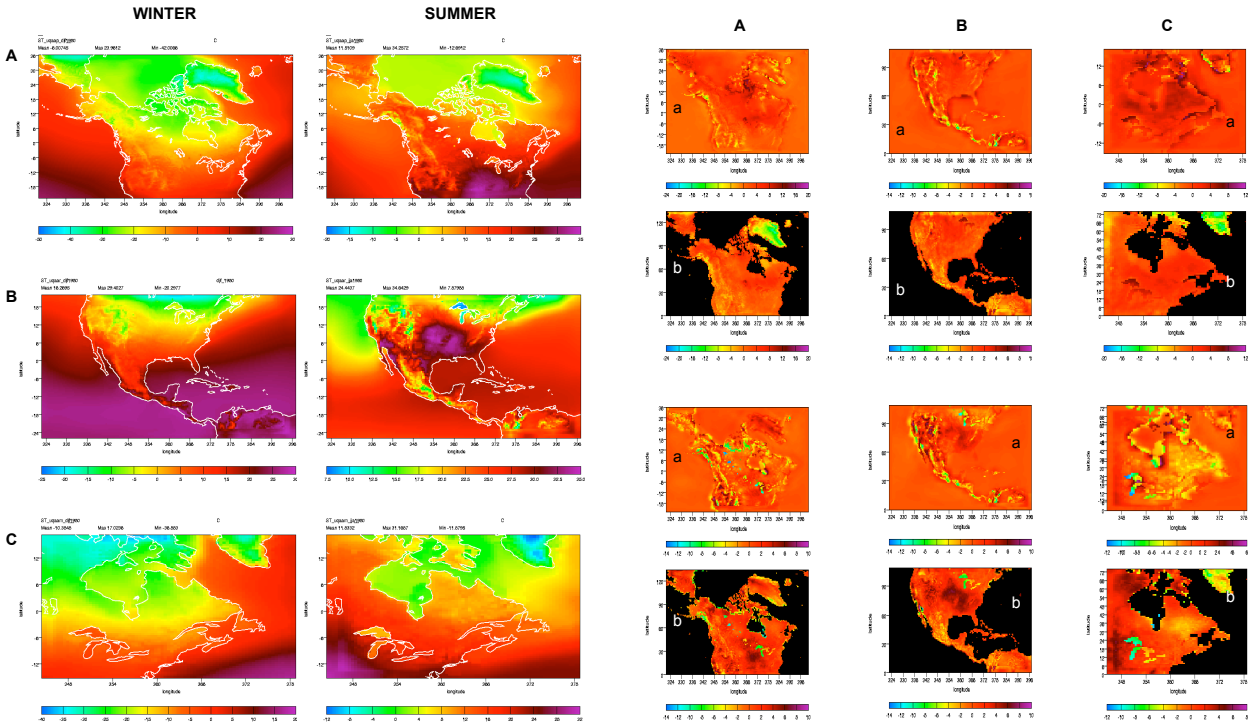

Fig. 2. Left panels: Winter (DJF) and Summer (JJA) mean temperature at 1.5m (°C) for the year 1980 as simulated by PRECIS, as nested data by ECMWF Reanalysis data (ERA), and analysed by CRU (Mitchell *et al*. 2004) for the three different domains, i.e. (A) Pan-Canada (180x135), (B) Central-America and USA (135x110) and (C) eastern North America (79x75). Right panel s: "PRECIS-ERA" (a) represents the added-value of the high resolution (0.44°), while "PRECIS-CRU" (b) presents the skill of PRECIS, for the three domains, A, B and C.

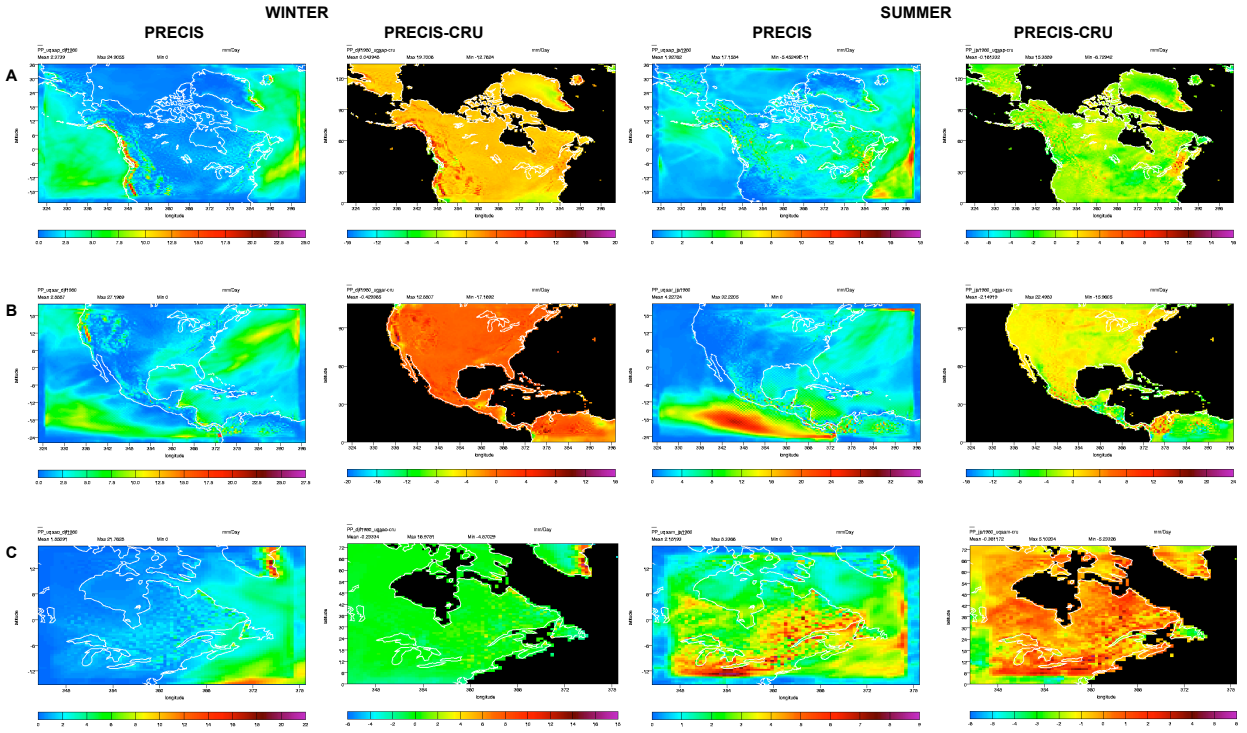

Fig. 3. Winter (DJF) and Summer (JJA) mean total precipitation rates (mm/day) for the year 1980 simulated by PRECIS and analysed by CRU (Mitchell *et al*. 2004) over the (A) pan-Canadian, the (B) central-America and USA, and (C) eastern North America domains. "PRECIS-CRU" represents the skill of PRECIS.

The author addresses her acknowledgments to Canadian Regional Climate Modelling Network and Ouranos that supported this initiative.

SPRING-SUMMER CLIMATE EXTREMES IN EURASIAN MIDLATITUDINAL REGIONS

I.I. Mokhov

A.M. Obukhov Institute of Atmospheric Physics RAS, Moscow, Russia
mokhov@ifaran.ru

Extremely dry and wet regimes in the Eurasian mid-latitudinal regions from the end of the XIX century to the beginning of the XXI century have been analyzed. In particular, statistically significant tendency of increase for the frequency and area of meteorological droughts during May-July (growing season) in the Eastern European (EER) and Western Asian (WAR) mid-latitudinal regions by data from (Meshcherskaya and Blazhevich, 1997) under the regional and hemispheric warming at the surface during last hundred years is noted (Mokhov, 2000; Mokhov et al., 2002). It is related to the statistically significant decrease of precipitation in spring and summer under the increase the surface air temperature both in EER and WAR though no statistically significant trends are found both for regional precipitation and for temperature during last century.

Table 1 shows parameters of temperature sensitivity of normalized precipitation (P) and indices of drought and extremely wet regimes (estimated by coefficients of appropriate linear regressions) during May-July by updated data from (Meshcherskaya and Blazhevich, 1997) for EER and WAR during 1891-2002. Index D characterizes the drought conditions with the negative precipitation anomalies δPr (normalized on the long-term mean value of precipitation) larger than -20% and positive temperature anomalies δT larger than 1K. Index M characterizes the wet conditions with $\delta Pr>20\%$ and $\delta T<-1K$. Two additional indices are used: D-M and $S=(\delta T/\sigma_{\delta T} - \delta P/\sigma_{\delta P})$, where $\sigma_{\delta T}$ and $\sigma_{\delta P}$ are respective standard deviations.

Table 1. Estimates of temperature sensitivity (with standard deviations) of normalized precipitation (P) and indices of drought and extremely wet regimes (D, M, D-M and S) for May-July from observations (1891-2002) in East European and West Asian mid-latitudinal regions (r – coefficient of correlation).

Sensitivity Parameters (1891-2002)	East European Region	West Asian Region
$D(P/P_o)/dT$, K^{-1} (r)	-0.08±0.01 (0.52)	-0.11±0.02 (0.58)
dD/dT, $\%K^{-1}$ (r)	11.1±0.7 (0.83)	12.7±0.8 (0.80)
dM/dT, $\%K^{-1}$ (r)	-9.2±0.7 (0.77)	-9.4±0.7 (0.79)
$d(D-M)/dT$, $\%K^{-1}$ (r)	20.3±0.9 (0.91)	22.1±1.0 (0.90)
dS/dT, K^{-1} (r)	0.72±0.03 (0.91)	0.77±0.03 (0.93)

According to Budyko et al. (1981), a remarkable increase of the droughts probability was expected from the analysis of different data in midlatitudinal Eurasian regions under the global warming at the end of the XX century. Observations show no statistically significant trends in drought regimes for EER and WAR during the last decades. It should be related with the regional changes in atmospheric circulation accompanying global warming during the last decades, and, in particular, related with changes of North Atlantic Oscillation and El-Nino phenomena (Mokhov, 2000). Figure 1 shows that probability of droughts during spring-summer in EER is less after positive anomalies of the sea surface temperature T_{Nino3} in January for the El-Nino formation region (Nino3) in the equatorial Pacific.

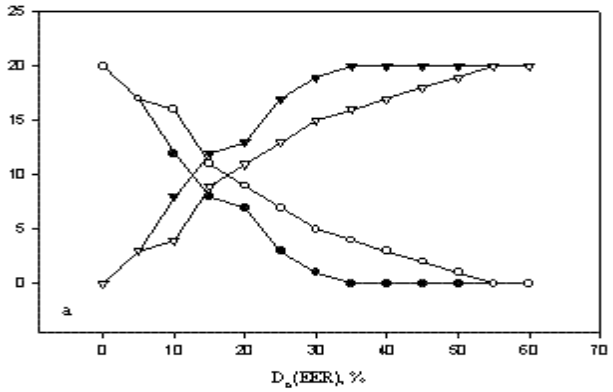

Fig. 1. Cumulative distributions of the number of years N_{cum} with $D>D_o$ (circles) and $D<D_o$ (triangles) for EER during 1950-1995: T_{Nino3}(January)>25.6°C (black) or T_{Nino3}(January)<25.2°C (white).

Cumulative distribution function $N_{cum}(D)$ can be approximated by an exponential function (similar to distributions for blocking characteristics). In particular, $N_{cum}(D)$ for EER is approximated by $N_o\exp[-(D/D_c)^2]$ slightly better than by $N_o\exp(-D/D_c)$. More detailed analysis of parameterization $N_{cum}(D)=N_o\exp(-D/D_c)$ shows different values of D_c for weak, moderate and strong droughts (D_c decreases with the increase of D).

This study was supported in part by the RFBR and RAS program.

References

Budyko, M.I., P.Ya. Groisman, O.A. Drozdov, and I.I. Mokhov, 1981: Climatic conditions of the next decade (1982-1991). 10 pp. (in Russian, unpublished)

Jones, P.D., and A. Moberg, 2003: Hemispheric and large-scale air temperature variations. *J. Climate,* **16,** 206-223.

Meshcherskaya, A.V., and V.G. Blazhevich, 1997: The drought and excessive moisture indices in a historical perspective in the principal grain-producing regions of the Former Soviet Union. *J. Climate,* **10,** 2670-2682.

Mokhov, I.I., 2000: Modelling of regional precipitation and river run-off for XX and XXI centuries. UNESCO Intern. School of Science for Peace "Global Climate Changes and Impact on Biosphere" Università degli Studi di Milano Bicocca, Milano (Italy), October 2-13, 2000.

Mokhov, I.I., J.-L. Dufresne, V.Ch. Khon, H. Le Treut, and V.A. Tikhonov, 2002: Regional regimes with drought and extreme wet conditions: Possible changes in XXI century from IPSL-CM2 simulations. *Research Activities in Atmospheric and Oceanic Modelling,* H. Ritchie (ed.), WMO/TD-No.1105, 07.31-07.32.

TERRESTRIAL BIOSPHERE RESPONSE TO ANTHROPOGENIC CHANGES IN GROWING SEASON IN EUROPEAN MID-LATITUDINAL REGIONS FROM MODEL SIMULATIONS

I.I. Mokhov (1), A.V. Chernokulsky (1,2), J.-L. Dufresne (3), H. Le Treut (3)

(1) Obukhov Institute of Atmospheric Physics RAS, Moscow, Russia
(2) Lomonosov Moscow State University, Moscow, Russia
(3) Laboratoire Meteorologie Dynamique du CNRS, Paris, France

mokhov@ifaran.ru

Regional droughts and terrestrial biosphere response to anthropogenic changes from simulations of a coupled atmosphere-ocean general circulation model IPSL-CM2 with a carbon cycle (Friedlingstein et al., 2001; Dufresne et al., 2002; Berthelot et al., 2002) for the 1860-2100 period are analyzed (Mokhov et al., 2002; Mokhov et al., 2004). According to (Mokhov et al., 2004) the increase of probability of meteorological droughts (expected in the XXI century) does not necessary lead to the decrease of the terrestrial biospheric productivity.

Model simulations are based on anthropogenic scenarios with the carbon dioxide emissions due to fossil and land use from observations up to 1990 and the IPCC SRES98-A2 emission scenario from 1990 to 2100. Different scenarios have been used, in particular the coupled scenario run (computed CO2 changes with A2-SRES scenario and computed climate), the control run (no CO2 emissions and computed climate) and the fertilization run (computed CO2 changes with A2-SRES scenario and climate changes from control run). In particular, changes of net primary production (NPP) and net ecosystem production (NEP) during growing season are studied. Model results are analyzed for European regions in the middle latitudes, in particular for Eastern European region (EER: 46.1-53.2N, 30.4-50.6E) and Western European region (WER: 46.1-53.2N, 0-11.2E) for growing season (May-July).

Figure 1(a,b) shows interannual changes of NPP (a) and NEP (b) in EER for growing season (May-July). Values of NPP and NEP from coupled (solid grey curves) and fertilization (broken grey curves) runs are normalized by their corresponding mean values in May-July for the 30-years period 1961-1990. Black curves display the 30-years running means for NPP and NEP. There is a general increase of NPP and NEP in the XXI century with the increase of their variability. The general increase of NPP and NEP in the coupled run is less than that in the fertilization run. So, the anthropogenic climate changes in EER lead to the decrease of NPP and NEP. The total rise of these values is due to CO2 increase.

Figure 2(a,b) similar to Fig. 1(a,b) shows corresponding changes of normalized values of NPP (a) and NEP (b) in EER. There is also a general increase of NPP and NEP in the XXI century with the increase of their variability. The variability of the normalized NPP is remarkably larger in EER than that in WER. It should be noted that the mean NPP values are remarkably larger in WER in comparison to EER. The difference of mean values for NEP in WER and EER is not so large as for NPP. The general increase of NEP in the coupled run is generally less than that in the fertilization run. Differences between two runs for NPP in WER are small but for the coupled run the NPP values are slightly larger than that for the fertilization run. The general increase of NPP and NEP in the coupled run is slightly larger than that in the fertilization run. So, the anthropogenic climate changes lead to the decrease of NEP and to the very little increase of NPP in WER.

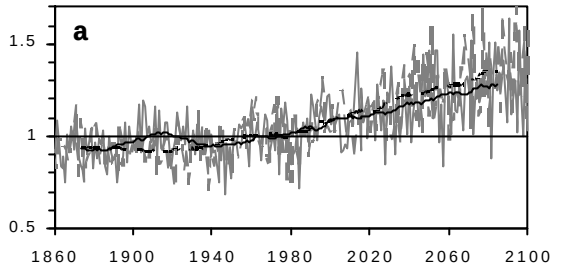

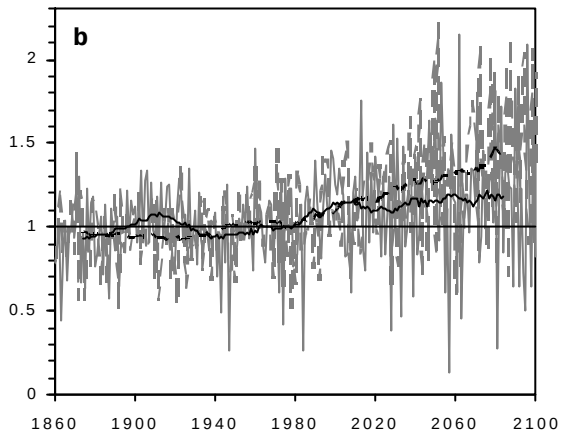

Fig.1. Changes of NPP (a) and NEP (b) in EER.

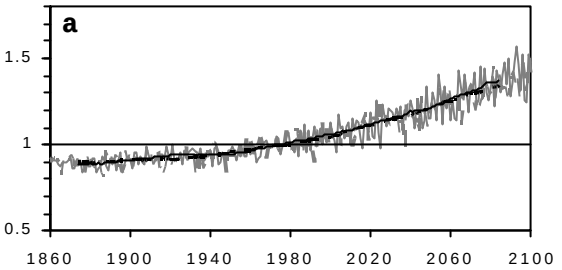

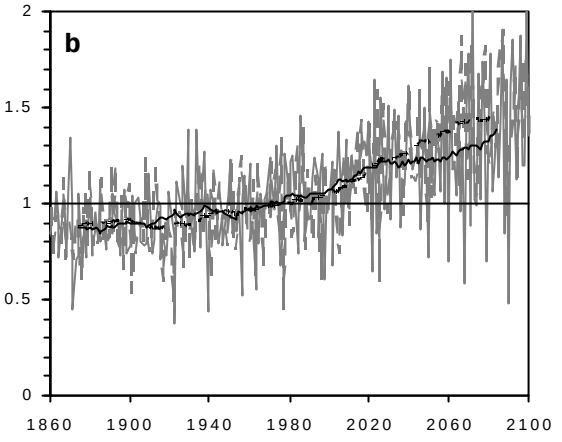

Fig.2. Changes of NPP (a) and NEP (b) in WER.

This work was supported by the CNRS/RAS Joint Agreement Program, RFBR and RAS Program.

References

Berthelot, M., P. Friedlingstein, P. Ciais, P. Monfray, J.-L Dufresne, H. LeTreut , and L. Fairhead,, 2002: Global response of the terrestrial biosphere to CO2 and climate change using a coupled climate-carbon cycle model. *Global. Biogeochem. Cycles*, **16**, 1084, doi:10.1029/.

Dufresne, J.-L., P. Friedlingstein, M. Berthelot, L. Bopp, P. Ciais, L. Fairhead, H. Le Treut, P. Monfray, J. Orr, 2002: Direct and indirect effects of future climate change on land and ocean carbon. *Geophys. Res. Lett.*, **29**, 1405, doi:10.1029/2001GL013777.

Friedlingstein P., L. Bopp, P. Ciais, J.-L Dufresne, L. Fairhead, H. LeTreut, P. Monfray, and J. Orr, 2001: Positive feedback between future climate change and the carbon cycle. *Geophys. Res. Lett.*, **28**, 1543-1546.

Mokhov, I.I., J.-L. Dufresne, V.Ch. Khon, H. Le Treut, and V.A. Tikhonov, 2002: Regional regimes with drought and extreme wet conditions: Possible changes in XXI century from IPSL-CM2 simulations. *Research Activities in Atmospheric and Oceanic Modelling, H. Ritchie (ed.)*, WMO/TD-No.1105, 07.31-07.32.

Mokhov, I.I., J.-L. Dufresne, H. Le Treut, and V.A. Tikhonov, 2004: Climate extremes and net primary production in Eastern Europe: Changes in XIX-XXI centuries from model simulations. *Research Activities in Atmospheric and Oceanic Modelling, J. Cote (ed.)*, WMO/TD-No.1220, 07.33-07.34.

Upstream Surface Heat flux Effects on the South China Sea Summer Monsoon

Xueli Shi[1,2], Johnny C. L. Chan[1*], K.C. Chow[1], and Yihui Ding[2]
[1]*Laboratory for Atmospheric Research, Department of Physics and Materials Science*
City University of Hong Kong, Hong Kong, China
[2.]*National Climate Center, China Meteorological Administration, Beijing, China*
*E-mail: Johnny.chan@cityu.edu.hk

1. Introduction

Sensitivity experiments of the upstream factors that could affect the South China Sea Summer Monsoon (SCSSM) onset and its subsequent evolution have been carried out using a regional climate model. The upstream regions here refer to the Bay of Bengal (BOB) and the two landmasses, i.e., the Indochina Peninsula (ICP) and the Indian subcontinent (IND). The factors include the sensible heat flux over the two landmasses and sensible heat flux over BOB.

2. Model and experiments design

The model used is the modified regional climate model developed by the National Climate Center of China and the City University of Hong Kong based on the NCAR RegCM2 (Ding et al. 2000; Chan et al. 2004). Three sensitivity experiments have been made here: cutting off only the latent heat flux over the BOB (BOBqfx), cutting off both the BOBqfx and the sensible heat flux over the ICP (BOBqfx+IChfx), and cutting off all the heat flux over the BOB, ICP and IND (BOBqfx+IChfx+INDhfx).

3. Results

Preliminary results show that removing the heat flux over the SCS upstream regions has great effects on the SCS, SC and the western North Pacific, with the effect becoming more significant as the region over which heat flux is cut off increases. A particular result is the prominent decrease of 850hPa westerlies over the SCS during the 3-6 pentads of May, which delays the onset of the SCSSM by 1-2 pentads (Fig.1). For the precipitation in May, a decrease in rainfall is found over the BOB and the adjacent coastal regions, as well as the southern tip of IND, Sri Lanka and parts of East China in BOBqfx (Fig. 2a). In BOBqfx+IChfx, the rainfall decrease region extends further downstream to SCS and South China, and the western North Pacific (Fig. 2b). The largest reduction in rainfall occurs in BOBqfx+IChfx+INDhfx (Fig. 2c). Despite such a quasi-linear relationship, the combined effect is not equal to (actually mostly less than) the sum of the individual effects, which suggests nonlinear interactions.

4. Concluding remarks

The results demonstrate the great of upstream heat flux and SST on the SCSSM. But only one simulation case has been made in our study without ensemble. And a coupled RCM with an ocean model may be necessary for better model performance.

Acknowledgments: This research was supported by the Research Grants Council of the Hong Kong Special Administrative Region Government of China Grant CityU 2/00C.

References

Chan JCL, Liu YM, Chow KC, Ding YH, Lau WKM, Chan KL. 2004. Design of a regional climate model for the simulation of South China summer monsoon rainfall. *Journal of Meteorological Society of Japan* (accepted).

Ding YH, Qian YF, Yan H, Gao K, Shen TL, Miao MQ, Li W, Liu YM, Zhao N, Yi L, Shi XL. 2000. Improvement of a high-resolution regional climate model and its application to numerical simulation of prolonged heavy rainfalls in East Asia. In Development of Operational Short-term Climate Model Series 2. Ding YH (Ed.). China Meteorological Press, Beijing, 217-231.

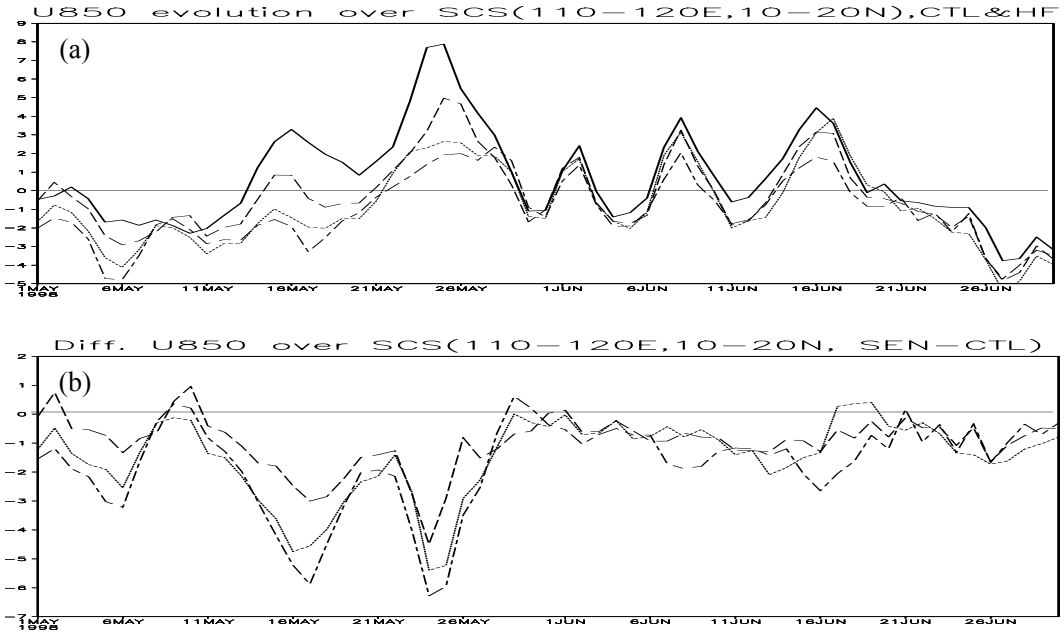

Fig.1 Time evolution of (a) 850 hPa zonal winds and (b) differences in 850-hPa zonal wind between the sensitivity experiments and the control experiment (CTL). All values are averaged over the region (10-20ºN, 110-120ºE). Unit: m s^{-1}. Solid line in (a): CTL, Long dashed line: BOBqfx, Dotted line: BOBqfx+IChfx, Long dashed, short dashed line: BOBqfx+IChfx+INDhfx.

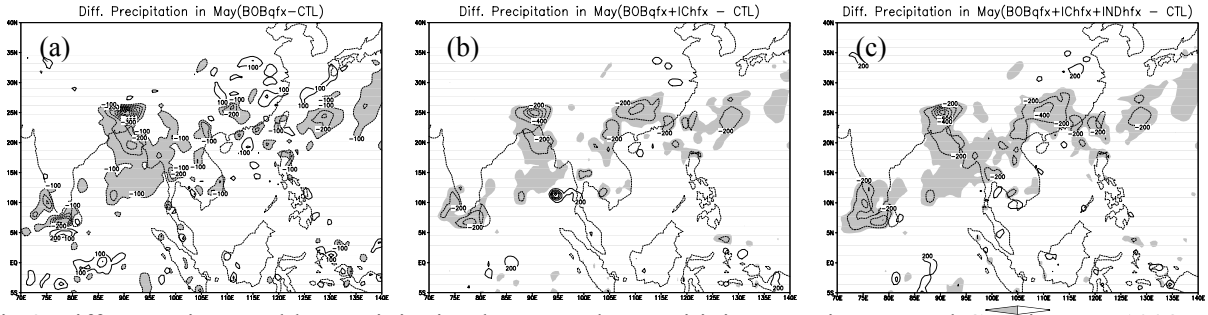

Fig.2 Difference in monthly precipitation between the sensitivity experiments and CTL in May 1998. (a) BOBqfx, (b) BOBqfx+IChfx, and (c) BOBqfx+IChfx+INDhfx. Unit: mm. Differences ≤ –100 mm are shaded.

The changes in precipitation characteristics during the Baiu (Mei-yu) season of the global warming climate simulated by a cloud-resolving non-hydrostatic regional model

*Kazuaki YASUNAGA[1], Yasutaka WAKAZUKI[1], Masanori YOSHIZAKI[2], Chiashi MUROI[2], Kazuo KURIHARA[2], Akihiro HASHIMOTO[1], Sachie KANADA[1], Teruyuki KATO[2]

[1]*Advanced Earth Science and Technology Organization, Tokyo*
[2]*Meteorological Research Institute / Japan Meteorological Agency, Tsukuba*

1. Introduction

We are trying to predict climate changes over East Asia during the rainy season in early summer (Baiu season), when greenhouse gas concentrations in the atmosphere increase, making use of a high-resolution nonhydrostatic model nested into a 20km-mesh AGCM.

Our previous paper (Yoshizaki et al. 2005) showed the precipitation during the Baiu season increases over the southern Japan islands, and decreases over the northern Japan Islands and the northern Korean Peninsula. It was also presented that the frequency of occurrence of heavy rainfall greater than 30 mm h^{-1} increases over the Japan Islands. However, there are two possibilities for the increase in the rainfall amounts and heavy rainfall frequency around the southern Japan islands in the warming climate simulation; (1) the Baiu front is long sustained in the warming climate simulation, or (2) precipitation characteristics associated with the Baiu front is changed. Therefore, in the present study, the changes of precipitation characteristics over East Asia are examined.

2. Model descriptions and experimental designs

A nonhydrostatic model named JMA-NHM, which has been jointly developed by the Meteorological Research Institute and the Numerical Prediction Division, Japan Meteorological Agency, is employed as a regional climate model. The JMA-NHM has been utilized for short-term predictions and climate simulation, and good model performances have been confirmed, especially for the forecast of heavy rainfall (Wakatsuki et al. 2004). The JMA-NHM is detailed in Saito et al. (2001).

The horizontal grid size of the regional climate model is 5 km, and the domain covers an area of 4000 km x 3000 km (Fig. 1). The model has 48 layers in the stretched vertical, with the finest resolution (20m) near the surface, and the coarsest resolution (920m) at the model top. Rayleigh damping is imposed near the upper boundary. Although a horizontal grid of 5 km can not fully resolve convective updrafts, the JMA-NHM with a horizontal grid of 5 km has successfully reproduced many heavy rainfall events, making use of explicitly represented cloud microphysics only (e.g., Kato 1998, Kato and Goda 2001). Therefore, no convective parameterization is used in the present study.

*Corresponding author address: Kazuaki Yasunaga, Meteorological Research Institute, 1-1 Nagamine, Tsukuba, Ibaraki 305-0052 Japan: e-mail: kyasunag@mri-jma.go.jp

The initial and lateral boundary conditions of the regional climate model, JMA-NHM were obtained from the outputs of the AGCM. In order to couple the AGCM and NHM smoothly, a spectral boundary coupling (SBC) method was adopted (Kida et al. 1991; Yasunaga et al. 2004). The SBC method is applied to the fields of horizontal winds and temperature above a height of 5km every 20 minutes. The SST is same as used in the AGCM. Since our goal is to predict climate changes during the Baiu season around East Asia, the simulation period is set as June and July.

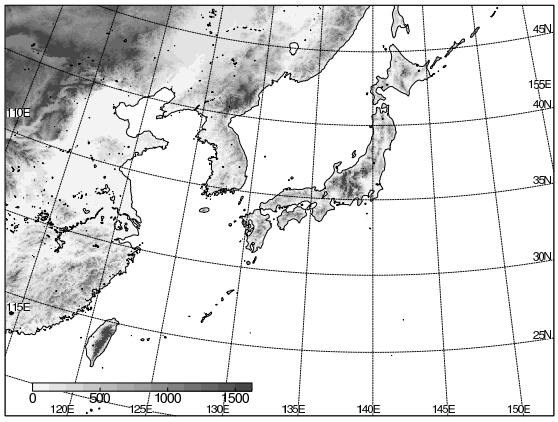

Fig. 1: The domain and orography of the JMA-NHM.

3. Results

Figure 2 represents accumulated rainfall amounts and normalized frequencies of precipitation over the model domain in June and July. The first 10 days data and data within 500 km of the nearest boundary are excluded in order to remove the influence of the initial fields and lateral boundary. While the rainfall amounts in June of the warming climate simulation agree with those in the present climate simulation, more rainfall is brought about in July of the warming climate simulation (Fig. 2a). The frequency of precipitation in the warm climate simulation greatly increases from that in the present climate simulation with intensity of the rainfall in July, although there are little differences in precipitation frequencies in June of between the present and warming climate (Fig. 2b).

In order to investigate how large precipitation systems mainly bring about rainfall over East Asia during June and July, the precipitation systems are classified according to area of the system (Fig. 3). The area of a precipitation system is calculated from aggregates of

precipitation grids connected with each other to north-south or east-west directions. The precipitation grid is defined as the intensity of the rainfall greater than 1 mm hr^{-1}. In this analysis, hourly outputs are used, and the continuity between the outputs is not considered.

Number of the precipitation system in the warm climate simulation agrees with that in the present climate simulation during June and July, except for that with the area of lager than 90000 km^2 in July (Fig. 3a). The precipitation systems with the lager area bring about more rainfall in June (Fig. 3b). There is also a large difference in the rainfall amounts from the precipitation systems with the area of lager than 90000 km^2 in July of the present and warming climate simulations (Fig. 3b). The precipitation systems with the area of lager than 90000 km^2 more frequently develop, and lead to more rainfall amounts in July in the warming climate than in the present climate. Moreover, it can be thought that the increase of the precipitation systems with the area of lager than 90000 km^2 results in the increase of the heavy rainfall event in July of the warming climate (Fig. 2b).

The precipitation systems with the area of lager than 90000 km^2 are most frequently observed around 30-40° N, 127-138° E in July of the warm climate (not shown). These precipitation systems are classified into sub-synoptic or meso-alpha-scale cloud systems, which are associated with relevant cyclonic circulation systems. The baroclinicity is deeply connected with the development of the cyclonic circulation systems, although condensation heating also plays the important role. The north-south gradient of the equivalent potential temperature around 30-40° N, 127-138° E is steeper in July of the warm climate than that in July of the present climate (not shown). The stronger baroclinicity in July of the warm climate simulation is consistent to the increase of the precipitation systems with the area of lager than 90000 km^2.

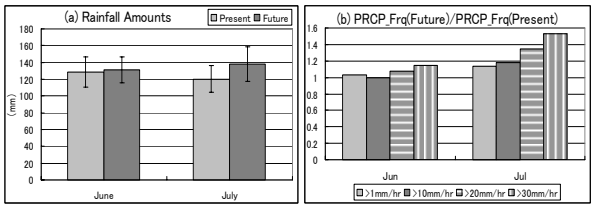

Fig.2: (a) Accumulated rainfall amounts, and (b) precipitation frequency in the warming climate normalized by that in the present climate over the model domain in June and July. In (a), light and dark gray columns denote the results in the present and warming climate simulation, respectively. Vertical lines show ranges within one standard deviation. In (b), light gray, dark gray, lateral stripe, and vertical stripe columns denote the normalized frequency of precipitation with the intensity of the rainfall greater than certain thresholds (1 mm hr^{-1},10 mm hr^{-1}, 20 mm hr^{-1}, and 30 mm hr^{-1}), respectively.

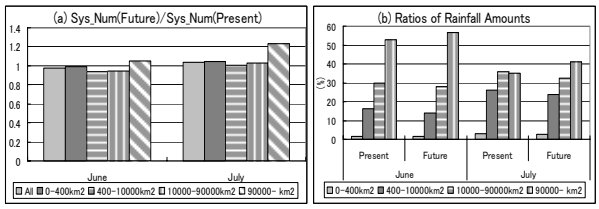

Fig.3: (a) Number of the precipitation systems with the certain size in the warming climate normalized by that in the present climate, and (b) ratios of the rainfall amounts brought about by the precipitation systems with the certain area to total rainfall amounts over the model domain in June and July. In (a), light gray, dark gray, lateral stripe, vertical stripe, and slanting stripe columns denote the normalized number of all precipitation systems and the systems with the area of 0-400 km^2, 400-10000 km^2, 10000-90000 km^2, and 90000- km^2, respectively. In (b), light gray, dark gray, lateral stripe, vertical stripe also show the ratios of the rainfall amounts from the precipitation systems with the area of 0-400 km^2, 400-10000 km^2, 10000-90000 km^2, and 90000- km^2, respectively.

Acknowledgements

This study is conducted by the fund of Research Revolution 2002, and the numerical calculations are made by NEC SX-6 on Earth Simulator.

References

[1]Deardorff, J. W., 1980: Numerical investigation of neutral and unstable planetary boundary layers. *Boundary-Layer Meteorol.*, **18**, 495-527.

[2]Kato, T., 1998: Numerical simulation of the band-shaped torrential rain observed over southern Kyushu, Japan on 1 August 1993. *J. Meteor. Soc. Japan*, **76**, 97-128.

[3]Kato, and Goda, 2001: Formation and Maintenance Processes of a Stationary Band-shaped Heavy Rainfall Observed in Niigata on 4 August 1998. *J. Meteor. Soc. Japan*, **79**, 899-924.

[4]Saito, K., T. Kato, H. Eito and C. Muroi, 2001: Documentation of the Meteorological Research Institute / Numerical Prediction Division Unified Nonhydrostatic Model. *Tech. Rep.of MRI*, **42**, p133.

[5]Wakazuki, Y. et al. 2004: Numerical experiment of climate change caused by global warming with the 5-km horizontal grid non-hydrostatic regional model. (2) Evaluation of the prediction accuracy and heavy rainfall frequency (in Japanese). *Prep. Autumn Meeting Meteor. Soc. Japan*, **86**, 147.

[6]Yasunaga, K., H. Sasaki, Y. Wakazuki, T. Kato, C. Muroi, A. Hashimoto, S. Kanada, K. Kurihara, M. Yoshizaki and Y. Sato, 2004a: Performance of the long-term integrations of the Japan Meteorological Agency nonhydrostatic model with use of the spectral boundary coupling method. Submitted to *Weather and Forecasting*.

[7]Yoshizaki, M. et. al. 2005: Changes of Baiu (Mei-yu) frontal activity in the global warming climate simulated by a cloud-resolving non-hydrostatic regional model. *SOLA* (*submitted*)